Measurement of PGE_2

PGE_2 (EIA kit-monoclonal; Cayman) concentrations were measured in the cell-culture supernatants in accordance with the manufacturer's instructions.

Statistical analysis

Statistical analyses were performed using GraphPad Prism software to calculate the means and SEMs. Group means were compared by using one-way analysis of variance (ANOVA), followed by Bonferroni's multiple comparison post test to identify statistically significant differences (i.e. $P < 0.05$).

Results

Gross histologic findings

Figure 1 shows the histologic features of ankle joints of Tg197 mice in the untreated, P-NT.II-treated, and scrambled-P-NT.II-treated groups. Gross histologic findings of the three experimental groups are summarized in Table 1. At 8 weeks of age, ankle joints from the untreated Tg197 group were moderately (90% with HS 3) to severely (10% with HS 4) damaged, with pannus and fibrous tissue formation and focal subchondral bone erosion. Articular cartilage destruction and bone erosion were observed in 90% of those joints (Fig. 1a,1b). In contrast, all the articular cartilage surfaces and associated synovial linings of the ankle joints of the P-NT.II-treated group at 2 weeks post-treatment (i.e. age 6 weeks) were only mildly affected (HS 2), with no evidence of cartilage or bone erosion (Fig. 1c), and 25% of joints were affected moderately (HS 3) at 4 weeks post-treatment (i.e. age 8 weeks) (Fig. 1d). In contrast, 83.3% of joints of scrambled-P-NT.II-treated Tg197 mice at 8 weeks of age were moderately damaged (HS 3) (Fig. 1e,1f), with histologic features similar to those of the untreated Tg197 mice. Although the disease, as assessed by the HS, was significantly lower in the P-NT.II-treated group than in the untreated or scrambled-P-NT.II-treated groups, visual disease scores (ASs) did not correlate well with the HS. In contrast to HSs, ASs of mice treated with P-NT.II did not significantly differ from those of the untreated or scrambled-P-NT.II-treated group (Fig. 2).

Analytical HS

To assess specific effects of the peptide P-NT.II on synovitis, cartilage destruction, and bone erosion, we conducted a semiquantitative scoring analysis for each of these pathologic parameters. P-NT.II treatment in Tg197 mice resulted in a significant reduction ($P < 0.05$) in all three analytical HSs as compared with those of untreated or scrambled-P-NT.II-treated Tg197 mice, which all developed synovitis with severe articular cartilage degradation and bone erosions (Fig. 3). Statistical analysis revealed a greater beneficial effect of P-NT.II on cartilage destruction and bone erosion (**$P < 0.01$ versus untreated or scrambled-P-NT.II-treated groups for both parameters) than on synovitis (*$P < 0.05$ versus untreated or scrambled-P-NT.II-treated groups).

Ultrastructural changes in articular cartilage

Articular cartilage in the ankle joints of all untreated Tg197 mice was generally damaged at 8 weeks of age (Fig. 4c,4d,4e,4f) as compared with normal morphology seen in control, wild-type mice (Fig. 4a). No significant ultrastructural changes in the nucleus and plasma membrane were noted at the cellular level in the articular cartilage of untreated Tg197 mice at age 4 weeks (baseline) except for some minor changes including vacuoles, dilated cisternae, and the presence of granular materials seen inside the cytoplasm (Fig. 4b). In the 8-week-old mice, the chondrocytes on the surface of the superficial cartilage layer had become necrotic, with alterations of cartilage developed in most cases (Fig. 4c,4d,4e,4f). The cell body and nucleus of some chondrocytes became large and rounded, resulting in vacuolation, and the cytoplasm was transparent, with an accumulation of intracytoplasmic filaments (Fig. 4c). Degenerating chondrocytes with greatly vacuolated cytoplasm and pyknotic nuclei (Fig. 4d), and chondrocytes with complete loss of nuclei and disrupted rough endoplasmic reticulum (r-ER) (Fig. 4e,4f), were also observed. In contrast, the ultrastructural features of chondrocytes 1–4 weeks after P-NT.II treatment (i.e. age 5–8 weeks; Fig. 5a) did not substantially differ from those seen in the joints of normal wild-type mice (Fig. 4a). Most of them had a prominent nucleus, lined by plasma membrane with short cytoplasmic protrusions, and vacuoles, r-ER, and mitochondria in the cytoplasm. The ultrastructure of chondrocytes of the scrambled-P-NT.II-treated joints at 8 weeks of age (Fig. 5b) were more or less similar to those described for untreated Tg197 mice with degenerating features such as the greatly vacuolated cytoplasm and pyknotic nuclei (cf. Fig. 4d) or loss of nucleus, disrupted r-ER (cf. Fig. 4f), and swollen mitochondria with distorted cristae (cf. Fig. 4c).

Ultrastructural changes in synovium

The early response of the synovial membrane in the untreated Tg197 mice at age 4 weeks (baseline) was synovial hyperplasia, with the presence of type A and B synovial cells along with inflammatory cells such as lymphocytes, macrophages, and mast cells. Type A cells were similar to macrophage cells and were characterized by many vesicles, vacuoles, and a higher number of cell processes. Type B cells were similar to fibroblast cells and contained small vesicles and r-ER. The later response (at ≥ 5 weeks of age) included degeneration of synovial cells, with swollen mitochondria and cell fragmentations. In areas of high inflammation, the synovial tissue (mostly type A cells) had proliferated into the articular cavity (Fig. 6a). Type A and B cells in the synovium were no longer distinguishable at age 6 weeks and thereafter. The synovial membrane was lined by closely packed elongated synoviocytes which

Figure 1

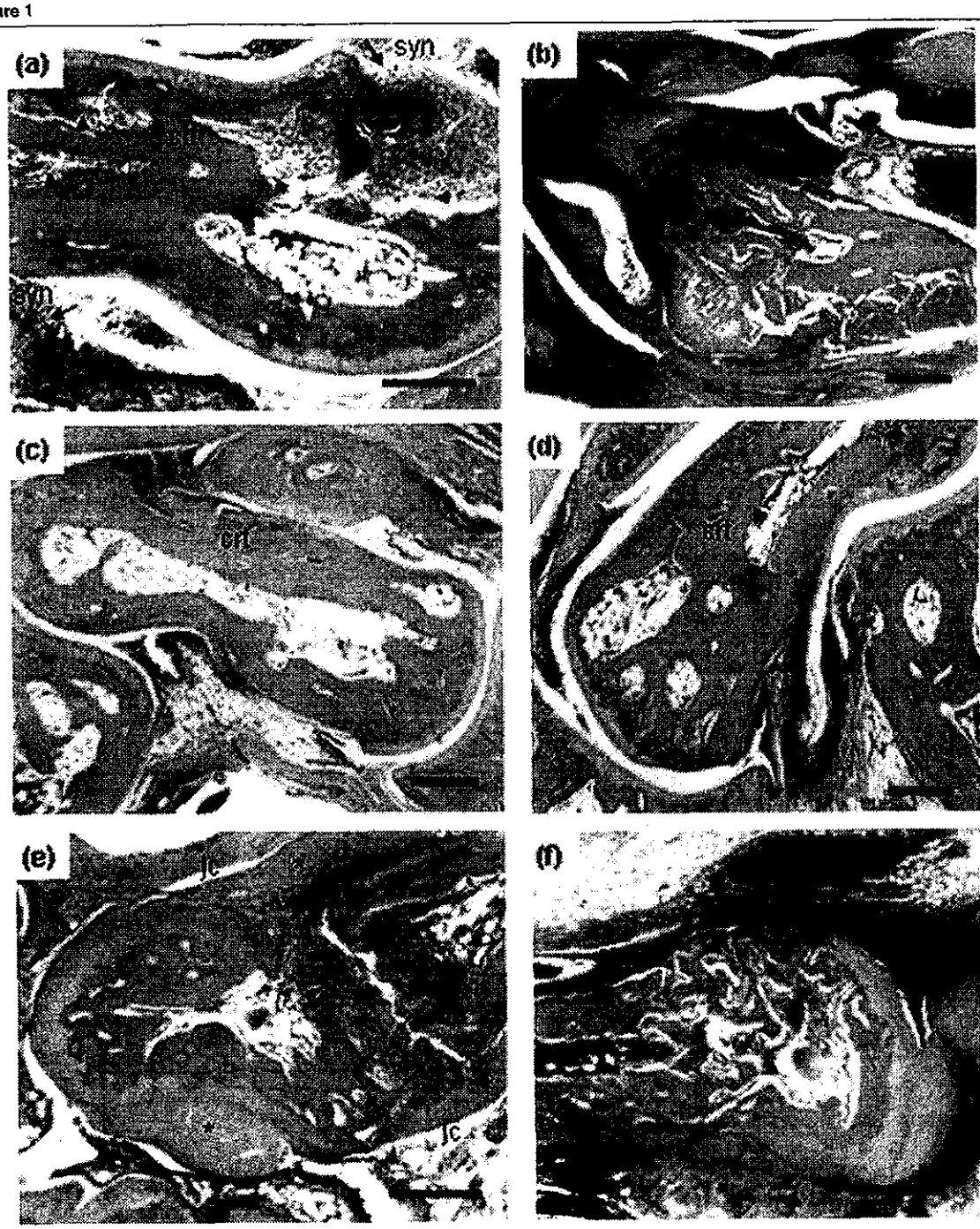

Histologic findings in the ankle joints of Tg197 mice. **(a,b)** Untreated mice: (a) partially altered articular cartilage (crt) with bone erosion (arrowhead), and presence of inflammatory infiltrates (arrow) in the synovial (syn) tissue; (b) extensive articular cartilage destruction and bone erosion (arrowhead). **(c,d)** P-NT.II-treated mice: (c) minor cartilage changes (crt) with absence of bone erosion; (d) focal articular cartilage destruction (crt) and minor bone erosion (arrowhead). **(e,f)** Mice treated with scrambled P-NT.II: (e) the joint cavity (jc) is lined with synovitis (*); (f) cartilage destruction and bone erosion (arrowhead) are present, along with inflammatory infiltrates (arrow). Nontransgenic controls showed normal joint structures throughout the study (data not shown). (Hematoxylin & eosin staining; original magnification ×25 in a, e, f; ×10 in b, c, d. Bars = 500 μm).

Table 1

Histopathologic assessment of ankle joints

Treatment	Time course (weeks)	Joints scored	% of total at indicated HS			HS (Mean ± SEM)
			HS 2	HS 3	HS 4	
None	4	10	0	90.0	10	3.30 ± 0.11[a]
P-NT.II*	1	4	100	0	0	2.12 ± 0.12
P-NT.II*	2	4	100	0	0	2.37 ± 0.12
P-NT.II*	3	4	75	25	0	2.50 ± 0.20
P-NT.II*	4	4	75	25	0	2.62 ± 0.31[b]
Scrambled-P-NT.II-treated (negative control peptide)	4	6	16.7	83.3	0	3.25 ± 0.17[c]

*Tg197 mice injected (intraperitoneally) with the test peptide P-NT.II were killed at weekly intervals ($N = 4$ per group) for 4 weeks and their ankle joints examined. For untreated and negative control groups, ankle joints were harvested only at the end of the 4 weeks' study course for one-time examination. Histologic scoring was performed semiquantitatively by a blinded examiner. HS 2 = pannus and fibrous tissue formation and focal erosion of subchondral bone; HS 3 = articular cartilage destruction and bone erosion; HS 4 = extensive articular cartilage destruction and bone erosion. *a* versus *b*, *b* versus *c* = significantly different ($P < 0.05$; one-way analysis of variance with Bonferroni's multiple comparison test). HS, histopathologic score; SEM, standard error of the mean.

were sealed by junctional systems of the adherent type (Fig. 6b). Large amounts of fibrin deposition on the synovial surface could be seen, and the two opposing, flattened synoviocytes with fibrin between them indicated the existence of synovial adhesion (Fig. 6d). Also, degenerating synoviocytes with disintegrating nuclei and vacuolated cytoplasm were randomly seen in the synovium (Fig. 6c). Synoviocytes appeared flattened, and partially degranulated mast cells were seen under the synovium (Fig. 6e).

P-NT.II treatment tended to decrease the number of inflammatory cells, with less degeneration of synovial cells and cell fragmentation seen in the joints of the treated group (Fig. 7b). The peptide P-NT.II retained at least the basic structural organization of the synovial membrane seen in the control wild-type mice (Fig. 7a), while the synoviocytes from mice treated with scrambled P-NT.II (Fig. 7c) were structurally indistinguishable from those seen in untreated joints (cf. Fig. 6). In those joints, the synovial cells were seen lining up close together, and many cell fragments resulting from degenerating cells were present in the synovium, along with infiltrating mast cells (Fig. 7c).

Serum levels of $sPLA_2$

In a time-course study to evaluate the specific effect of peptide in modulating the serum $sPLA_2$ levels in Tg197 mice (Fig. 8), P-NT.II significantly suppressed the circulating $sPLA_2$ in the mice at age 8 weeks ($P < 0.05$), by comparison with the serum levels of the untreated mice of same age. In contrast, the circulating $sPLA_2$ of scrambled-P-NT.II-treated and untreated Tg197 mice at age 8 weeks were not significantly different ($P > 0.05$), thus indicating the specific effect of the peptide P-NT.II on $sPLA_2$ levels.

PGE_2 release from cultured macrophages

The suppressive effect of P-NT.II and $sPLA_2$-selective inhibitor LY315920 (Lilly) on LPS- and TNF-stimulated PGE_2 production was examined in mouse macrophage cell cultures (Fig. 9). Production of PGE_2 in the medium increased approximately sixfold from the basal level of 55 ± 6 pg/ml to 320 ± 35 and 330 ± 11 pg/ml (mean ± SD, $N = 5$), after 20 hours' stimulation of cultured cells with LPS (2 μg/ml) (Fig. 9a) or TNF (10 ng/ml) (Fig. 9b), respectively. When the inhibitors were coincubated with either LPS- or TNF-stimulated macrophages in the medium, both P-NT.II and LY315920 (final concentration 10 μM) dose-dependently inhibited PGE_2 production, with estimated IC_{50} values of 25 and 30 μM, respectively. In contrast, scrambled P-NT.II (negative control) showed no inhibitory effect on either LPS- or TNF-induced PGE_2 release in the culture medium. Neither the peptide nor LY315920 affected the cellular viability, when tested by XTT assay kit at the highest concentration (40 μM) used in culture experiments ($E_{492\,nm}$ values of 0.89 ± 0.02, 0.84 ± 0. 021, and 0.92 ± 0.019 for untreated, P-NT.II-treated, and LY315920-treated cells, respectively).

Discussion

Here we report the beneficial effect of peptide treatment, and the ultrastructural changes seen at the cellular level in the articular cartilage and synovium of the ankle joints of TNF transgenic Tg197 mice treated with the anti-inflammatory peptide P-NT.II. While several studies have previously been carried out on the early ultrastructural changes in other animal models of experimental arthritis [23-25], no morphological evaluations in this TNF transgenic mouse model of RA have yet been available, in either the absence or the presence of therapeutic intervention.

Figure 2

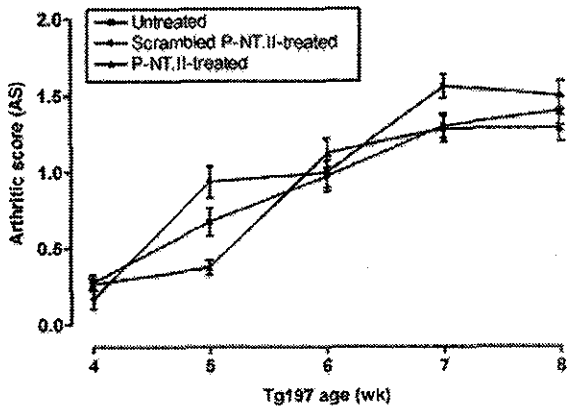

The arthritis score (AS) in Tg197 mice changes with time course. The AS was determined on both ankle joints of each mouse by a blinded examiner, using a scale of 0–3 as described in Materials and methods. Values are the mean ± SEM.

Figure 3

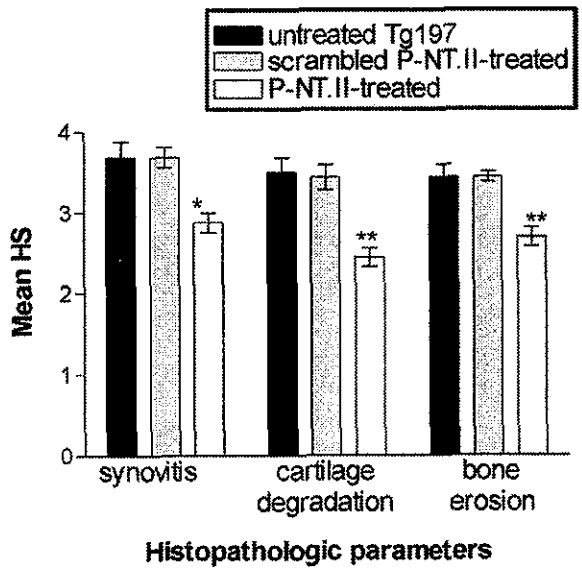

Histopathologic score (HS) analysis of various histopathologic parameters in Tg197 mice. Synovitis, cartilage degradation, and bone erosion were semiquantitatively assessed in the ankle joints of Tg197 mice that were untreated, treated with P-NT.II, or treated with scrambled-P-NT.II ($N = 4$/group) at 4 weeks post-treatment (i.e. age 8 weeks). The HS indicates a protective effect of P-NT.II in all three histopathologic parameters of arthritis. Statistical analysis revealed a greater beneficial effect of P-NT.II on cartilage destruction and bone erosion (**$P < 0.01$ versus untreated or scrambled-P-NT.II-treated groups for both parameters) than on synovitis (*$P < 0.05$ versus untreated or scrambled-P-NT.II-treated groups).

The lesions in the TNF transgenic mouse model of arthritis we used in the present study histologically and ultrastructurally resemble RA lesions [26], with synovial proliferation along the articular surface and subsequent invasion with erosion of the articular cartilage and subchondral bone. Although visual disease scores (ASs) did not show any significant difference between P-NT.II-treated and control (scrambled-P-NT.II-treated or untreated) groups, the results obtained from gross histologic analysis (Table 1) and semiquantitative analysis of pathologic parameters (Fig. 3) clearly demonstrate the beneficial effect of peptide treatment in preventing synovitis, cartilage destruction, and bone erosion. Similar discrepancies between AS and HS have also been reported in TNF-transgenic and other experimental models of arthritis. Redlich and colleagues [27] recently reported a protective effect of osteoprotegerin treatment on bone damage in Tg197 mice, with lack of any beneficial effect on the clinical symptoms. In another experimental model of passive collagen-induced arthritis using JNK2-deficient mice, it has been shown that clinical symptoms appear to be slightly more severe than HS despite significant reductions in joint destruction due to preservation of the articular cartilage [28]. It seems, therefore, that preservation of the bone structure may not always correlate with the clinical symptoms. The striking difference observed in the ultrastructural features of the articular cartilage and synovial membrane in our animal model before and after peptide treatment did confirm that P-NT.II administered as an exogenous drug in this TNF transgenic mouse model of RA was able to improve the overall morphology and the cellular component of the synovium, and of the cartilage in particular.

Ultrastructural changes of ankle articular cartilage and synovium in Tg197 mice were evaluated using transmission electron microscopy, before and during the 4-week course of treatment. Histologically, we observed an apparent suppression of pannus formation and minimal erosive damage to the articular cartilage and subchondral bone. At 1–4 weeks post-treatment with peptide (i.e. at age 5–8 weeks), the number of inflammatory cells in the synovial tissue was reduced as early as 1 week after initiation of treatment, and the structural organization of the synovial membrane of the ankle joint appeared less modified. In the P-NT.II-treated group, lesions such as synovial adhesions, cell fragmentation due to degeneration of synoviocytes, and dilation of the r-ER and distorted cristae of type B cells were less obvious than in the untreated or scrambled-P-NT.II-treated groups. In our cell-culture experiments using mouse macrophages, P-NT.II has been found to dose-dependently inhibit LPS- or TNF-induced PGE_2 production, with a potency equal to that of a potent and selective $sPLA_2$ inhibitor, LY315920 [29]. It is possible that P-NT.II may modulate ultrastructural modifications to the synovium by reducing the bioavailability of arachidonic acid (AA) through $sPLA_2$ inhibition, and

Figure 4

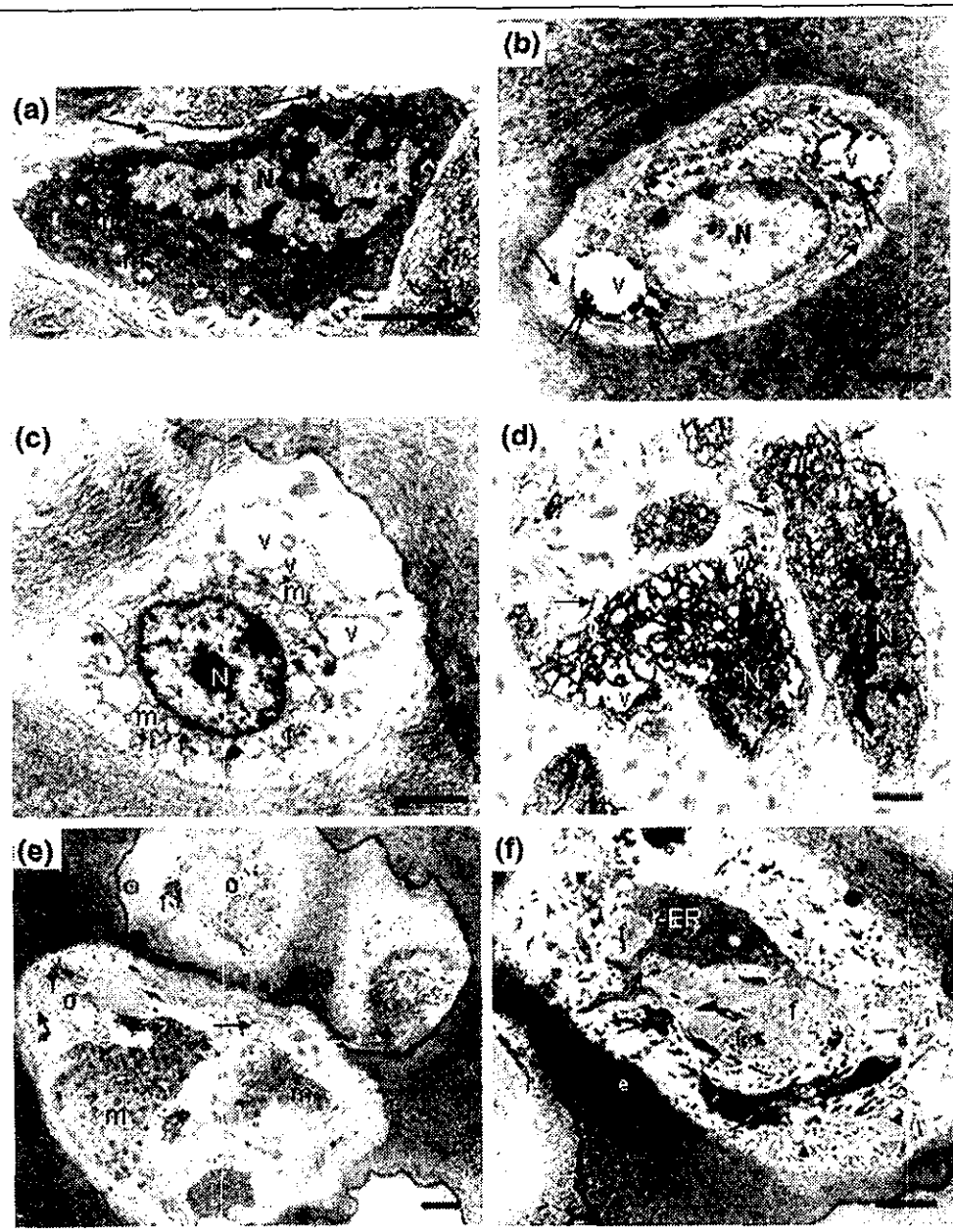

Chondrocytes of wild-type controls and untreated Tg197 mice. **(a)** Wild-type control at age 8 weeks: nucleus (N), plasma membrane with short cytoplasmic protrusions (arrow), rough endoplasmic reticulum (r-ER) (arrowhead), and mitochondria (m); **(b)** untreated Tg197 mouse at age 4 weeks: nucleus (N) and plasma membrane with cytoplasmic thin protrusions (arrow) appear normal, while the cytoplasm shows vacuoles (v) with granular materials inside (double arrow) and dilated cisternae (arrowhead). **(c-f)** Untreated Tg197 mouse at age 8 weeks: degenerating chondrocytes showing the following: (c) transparent cytoplasm with nucleus (N) and an accumulation of intracytoplasmic filaments (f), vacuoles (v) and mitochondria (m) with distorted cristae; (d) greatly vacuolated cytoplasm (v), and pyknotic nuclei (N) with cytoplasmic projections coming apart from the cell (arrow); (e) cell organelles from disintegrated cells (o), mitochondria (m), bundles of densely packed collagen fibres (arrowhead), small residues of intermediate filaments (f), and broken cellular processes (arrow); (f) swollen and disrupted r-ER, and bundles of thickened intermediate filaments (f). Basement membrane, cytoplasmic organelles (arrow), and cellular processes (arrowhead) were also fragmented. Electron-dense areas (e) are seen in the intercellular matrix. $N = 4$ joints; mean percentage of degenerating chondrocytes = 40% and 80% of total at 4 and 8 weeks of age, respectively. Bars = 2 μm.

Figure 5

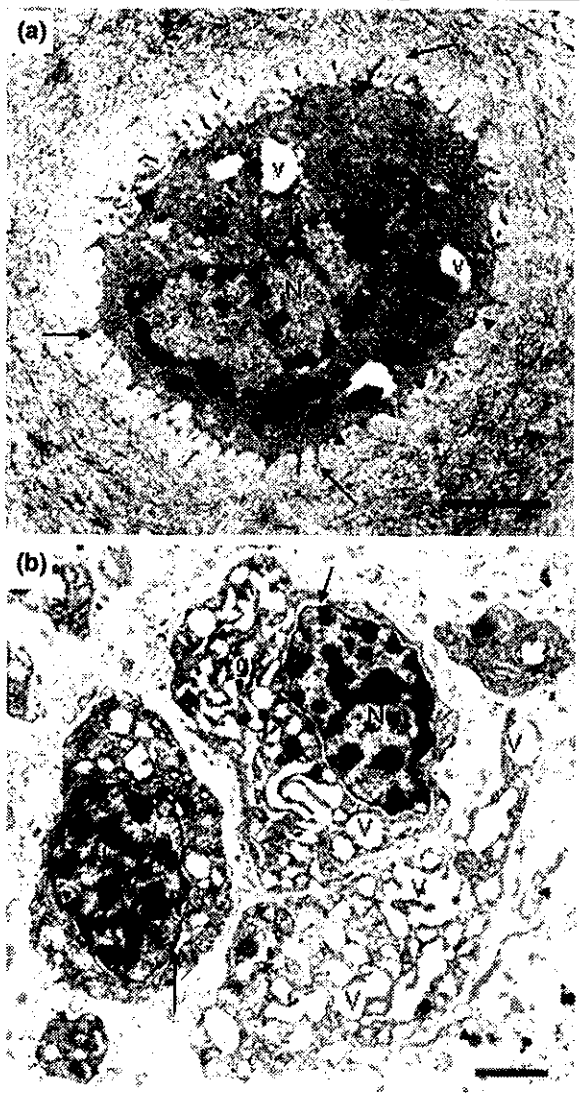

Chondrocytes of treated Tg197 mice. **(a)** Chondrocytes of P-NT.II-treated Tg197 mice at 5–8 weeks of age (i.e. 1–4 weeks post-treatment) were similar to those described for normal chondrocytes, with almost intact nucleus (N), basement membrane (arrowhead), and cytoplasmic organelles – vacuoles (v), rough endoplasmic reticulum (r-ER), mitochondria (m); **(b)** Most chondrocytes of Tg197 mice treated with scrambled P-NT.II at age 8 weeks (i.e. 4 weeks post-treatment) were degenerated, with vacuolated cytoplasm (v), a disrupted Golgi complex (g), pyknotic nuclei (N) with a well-defined, enlarged perinuclear space (arrows), and cytoplasmic projections broken from the cell (arrowhead). $N = 4$ joints/group; mean percentage of degenerating chondrocytes at age 8 weeks = 20% and 75% of total in (a) and (b), respectively. Bars = 2 μm.

suppress the severity of the prostaglandin-mediated inflammatory response in the synovium.

The ultrastructural features of the articular cartilage observed in this human TNF transgenic mouse model of RA suggest that the chondrocyte may be one of the important targets of the peptide intervention in modulating the progression of the joint erosion. Our extensive histopathologic analysis of joints in the Tg197 TNF model in this study (Fig. 3) has revealed both articular cartilage destruction and subchondral bone erosion at the advanced stages of disease (i.e. 8 weeks of age). Similar severe cartilage destruction in Tg197 mice at 7–8 weeks of age has previously been shown as evidenced by the loss of safranin-O staining [22]. Massive cartilage and subchondral bone erosion in the joints is the hallmark of inflammatory arthritis in the TNF transgenic mouse model [30]. At 3–4 weeks post-treatment (i.e. at 7–8 weeks of age), P-NT.II significantly reduced chondrocyte necrobiosis, which was frequently seen in the proximity of invading synovium in untreated controls at same age. It is possible that $sPLA_2$ might be involved in cartilage destruction in the TNF-transgenic model. $sPLA_2$ found in the synovial fluid has been reported to originate from chondrocytes and not from the synovial lining or inflammatory cells [31]. Human articular chondrocytes synthesize and constitutively release $sPLA_2$, and are therefore suggested to be responsible for the high concentration of $sPLA_2$ present in articular cartilage [32]. $cPLA_2$ is also reported to be involved in PGE_2 production by osteoblast cells [33], while there are reports indicating that $sPLA_2$ augments $cPLA_2$ expression in mouse osteoblasts via endogenous PGE [13,34]. Because of the significant functional coupling and/or synergism that can exist between $cPLA_2$ and $sPLA_2$ in various cells [3,13,33-35], $sPLA_2$ could conceivably be involved in chondrocyte destruction in RA by playing a role in bone resorption through crosstalk with $cPLA_2$.

We have found significantly elevated levels of circulating $sPLA_2$ in Tg197 mice at 8 weeks of age as compared with the much lower baseline levels detected at 4 weeks of age. Elevated levels of $sPLA_2$ have been reported in the plasma of patients with acute and chronic inflammatory diseases [36]. $sPLA_2$ can mobilize AA to induce the *de novo* synthesis of eicosanoids in a variety of inflammatory cells [37], leading to subsequent release of proinflammatory mediators. Recently, $sPLA_2$ has been shown to amplify TNF-induced PGE_2 synthesis in human rheumatoid synoviocytes [8], a process that is blocked by cyclic peptide inhibitors of human $sPLA_2$ [38]. The use of a low-molecular-weight peptide, such as P-NT.II, that effectively lowers $sPLA_2$ could be of clear clinical benefit in similar situations. Our results obtained with P-NT.II-treated Tg197 mice demonstrated that this new peptide inhibitor significantly suppressed the circulating $sPLA_2$ activity in those mice, whereas scrambled P-NT.II (negative control peptide) was without any effect.

Figure 6

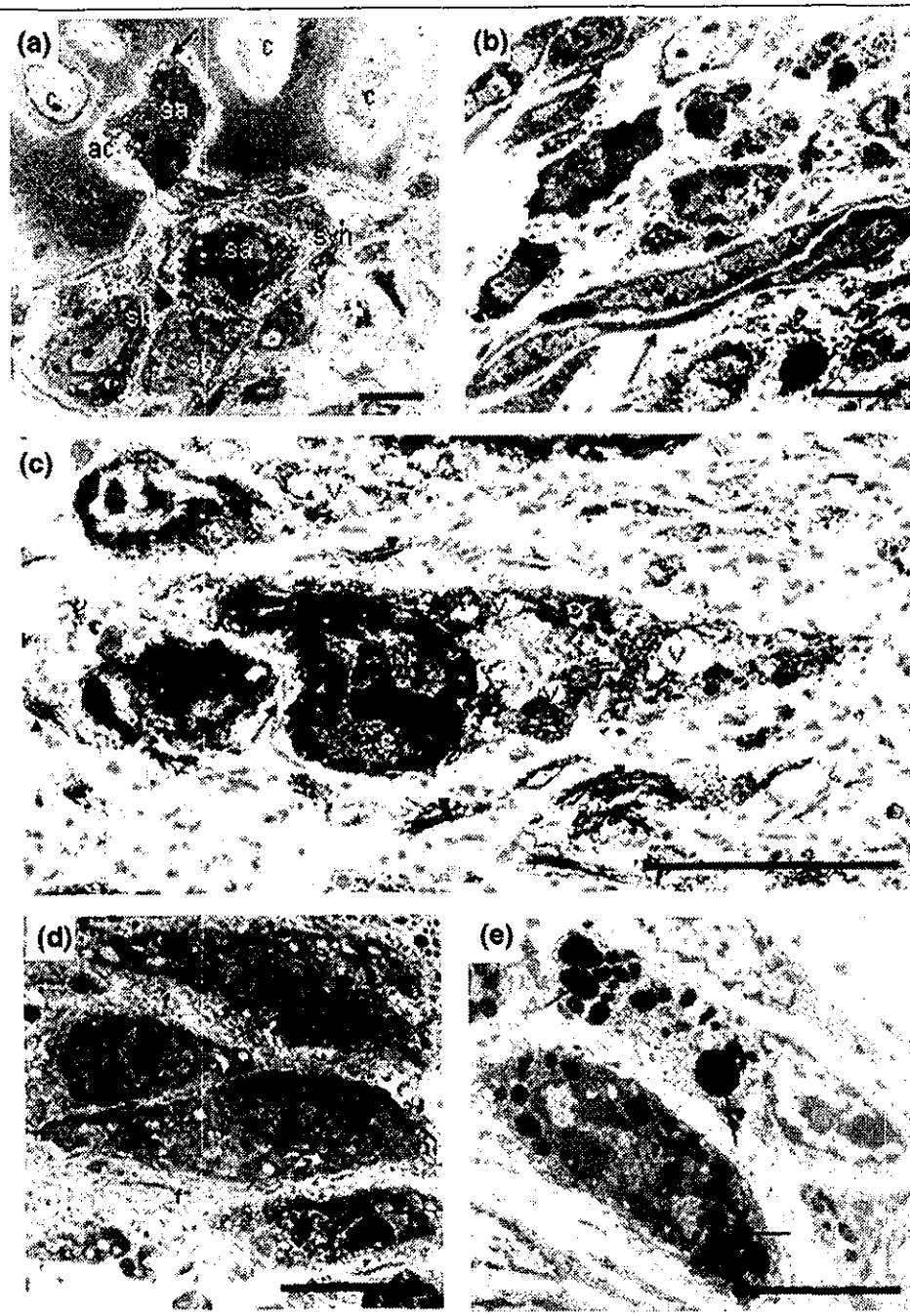

Synovium of untreated Tg197 mice at age 8 weeks. **(a)** Proliferation of the synovial tissue (syn) in the articular cavity (ac) showing macrophage-like type A synoviocytes (sa) with thin cytoplasmic protrusions (arrow) *invading the articular surface* (as), and closely packed secretory type B synoviocytes (sb) seen in the superficial layer of pannus. **(b)** The synovial membrane was lined by closely packed, elongated (arrow) or rounded synoviocytes with infiltrating cells (arrowhead) present under the synovium. **(c)** Degenerating synoviocyte with disintegrated nuclei (arrow) and vacuolated (v) cytoplasm along with disrupted collagen fibres (arrowhead) randomly seen in the synovium. **(d)** Adherent-type junction (arrow) sealing two synoviocytes with fibrin (f) between them. **(e)** Synoviocytes appeared flattened, and partially degranulated mast cells (arrow) are seen under the synovium. $N = 4$ joints; mean percentage of degenerating synoviocytes = 80% of total cells. Bars = 5 μm. c, chondrocytes; N, nucleus.

Figure 7

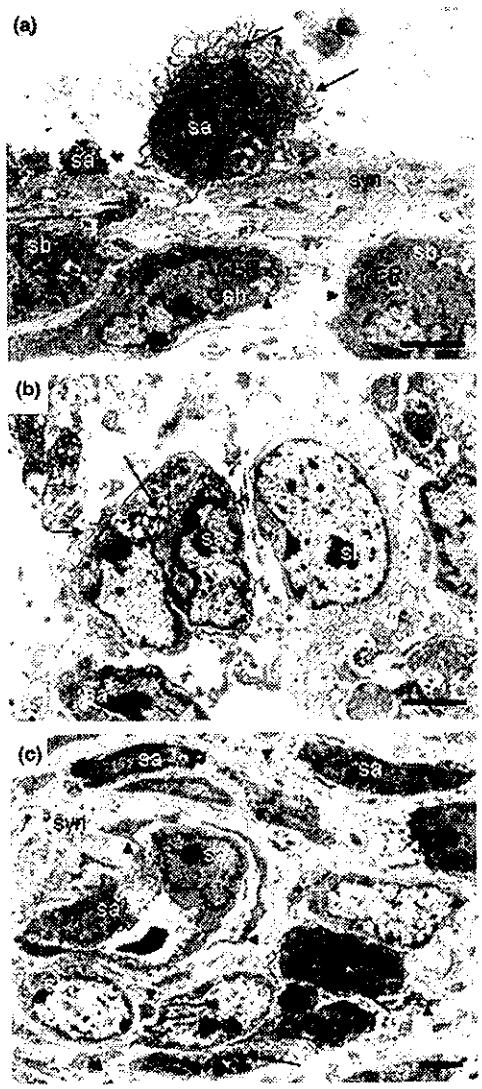

Synovium of treated Tg197 mice. **(a)** Nontransgenic wild-type group (control) at age 8 weeks: type A (sa) and type B (sb) synoviocytes are arranged loosely in the synovium (syn). Type A cells are characterized by many thin filopodia (arrow), while type B cells contain many instances of rough endoplasmic reticulum (r-ER), small vesicles, and basement membrane structures (arrowhead); **(b)** P-NT.II-treated Tg197 group at 5–8 weeks of age: synoviocyte A cells (sa) with characteristic cytoplasmic processes intermingled with those of neighboring cells (arrow) and B cells (sb), seen at age 6–8 weeks of age (i.e. 2–4 weeks post-treatment), appear unmodified during the time course (1–4 weeks) of treatment. The ultrastructural features are similar to those seen in the ankle joints of wild-type controls in (a). **(c)** Scrambled-P-NT.II-treated Tg197 group at age 8 weeks: type A (sa) and B (sb) synovial cells were seen lining up close together, and many cell fragments (arrowheads) resulting from fibrous degeneration of endothelial cells were present in the synovium (syn), along with infiltrating mast cells (arrows). $N = 4$ joints/group; mean percentage of degenerating synoviocytes = 24% and 75% of total in (b) and (c), respectively. Bars = 2 μm.

Figure 8

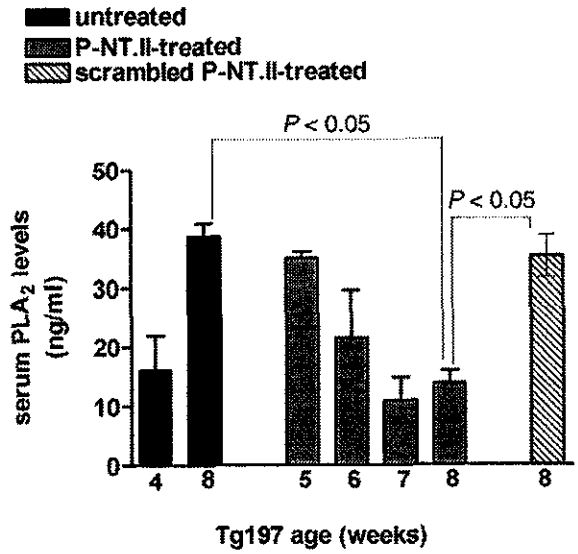

Time course of serum phospholipase A_2 ($sPLA_2$) levels. Serum $sPLA_2$ levels were measured with an *Escherichia coli* membrane assay in blood samples collected from untreated, P-NT.II-treated, and scrambled-P-NT.II-treated Tg197 mice at weekly intervals during the 4 weeks' time course of treatment. Values are the mean ± SD ($N = 4$/group). One-way ANOVA with Bonferroni's multiple comparison post test: $P < 0.05$, untreated versus P-NT.II-treated (age 8 weeks); $P < 0.05$, scrambled-P-NT.II-treated versus P-NT.II-treated (age 8 weeks).

The data obtained from the present study suggest that P-NT.II ameliorates synovitis and bone and cartilage erosions in the joints through modulation of circulatory and localized $sPLA_2$, which might otherwise amplify TNF-dependent pathways in rheumatoid synovium. Although the mode of action of $sPLA_2$ in this animal model is not exactly known, the potential mechanism may involve binding to a receptor [39], followed by internalization [40] and transfer of $sPLA_2$ to intracellular pools of phospholipids enriched in AA [41]. Further catalysis by $sPLA_2$ through surface interactions can then initiate and promote pathology by releasing AA, which can subsequently be converted to proinflammatory prostaglandins and leukotrienes. There are no published reports of $sPLA_2$ inhibitors showing benefit on bone erosion. The ultrastructural evidence of the beneficial effect of the peptide on joint destruction as shown here suggests a possible use of $sPLA_2$ inhibitors in the treatment of inflammatory bone loss diseases such as RA. However, some caution is advisable in the interpretation of the findings, since the nature of the arthritis in a purely TNF-driven disease, such as that observed in TNF transgenic mice, may not truly reflect the situation in human inflammatory joint diseases.

Conclusion

The present study provides ultrastructural demonstration of the modulatory effect of the P-NT.II peptide on synovial

Figure 9

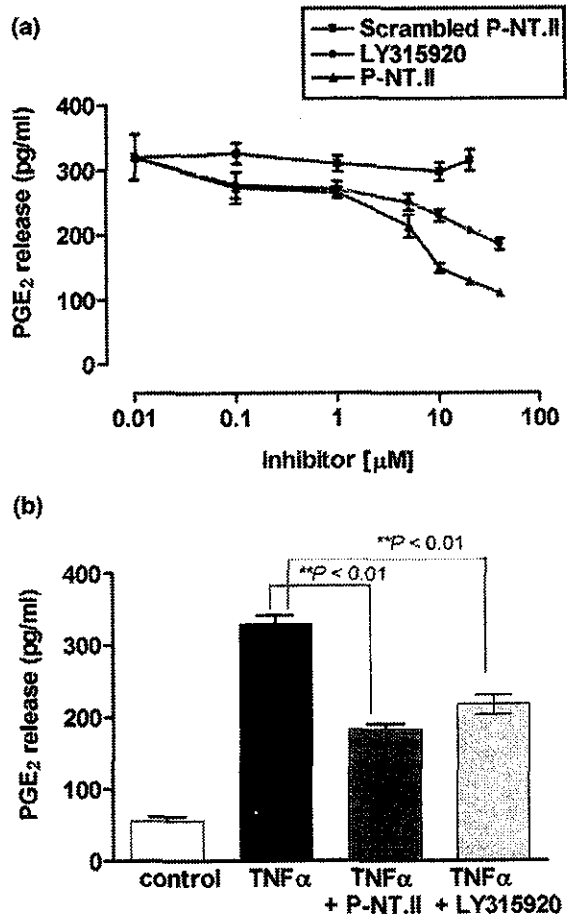

Modulation of lipopolysaccharide (LPS)- and tumor necrosis factor (TNF)-stimulated PGE_2 release. Macrophages (5×10^5 cells/ml) from subcultured J774 mouse cell line were incubated with **(a)** LPS (2 μg/ml) or **(b)** TNF (10 ng/ml) in the absence or the presence of various concentrations (0–40 μM) of P-NT.II, LY315920, or scrambled P-NT.II for 20 hours. Supernatants were collected, and PGE_2 release in the medium was determined by enzyme-linked immunosorbent assay. Results are shown as the mean ± SEM of five experiments performed in duplicate. $^{**}P < 0.01$ between inhibitor-treated and untreated cultures.

inflammation and joint destruction in TNF-driven Tg197 mouse model of human RA. The results suggest that $sPLA_2$ seems to play a significant role in inflammatory arthritis, and $sPLA_2$ inhibitors may be useful for the development of novel agents to treat RA and other inflammatory diseases.

Competing interests

None declared.

Acknowledgements

We are grateful to Mr Spiros Lalos and Ms Alexia Giannakopoulou, Institute of Immunology, Biomedical Sciences Research Centre, Al Fleming, Greece, and Ms Ng Geok Lan and Ms Chan Yee Gek, Department of Anatomy, Faculty of Medicine, National University of Singapore, for their excellent technical assistance.

References

1. Nevalainen TJ, Haapamaki MM, Gronroos JM: **Roles of secretory phospholipases A(2) in inflammatory diseases and trauma.** *Biochim Biophys Acta* 2000, **1488**:83-90.
2. Lin MK, Farewell V, Vadas P, Bookman AA, Keystone EC, Pruzanski W: **Secretory phospholipase A2 as an index of disease activity in rheumatoid arthritis. Prospective double blind study of 212 patients.** *J Rheumatol* 1996, **23**:1162-1166.
3. Huwiler A, Staudt G, Kramer RM, Pfeilschifter J: **Cross-talk between secretory phospholipase A2 and cytosolic phospholipase A2 in rat renal mesangial cells.** *Biochim Biophys Acta* 1997, **1348**:257-272.
4. Jamal OS, Conaghan PG, Cunningham AM, Brooks PM, Munro VF, Scott KF: **Increased expression of human type IIa secretory phospholipase A2 antigen in arthritic synovium.** *Ann Rheum Dis* 1998, **57**:550-558.
5. *Vadas P, Pruzanski W,* Kim J, Fox N: **The proinflammatory effect of intra-articular injection of soluble human and venom phospholipase A2.** *Am J Pathol* 1989, **134**:807-811.
6. Bomalaski JS, Lawton P, Browning JL: **Human extracellular recombinant phospholipase A2 induces an inflammatory response in rabbit joints.** *J Immunol* 1991, **146**:3904-3910.
7. Lin MK, Katz A, van den BH, Kennedy B, Stefanski E, Vadas P, Pruzanski W: **Induction of secretory phospholipase A2 confirms the systemic inflammatory nature of adjuvant arthritis.** *Inflammation* 1998, **22**:161-173.
8. Bidgood MJ, Jamal OS, *Cunningham* AM, Brooks PM, Scott KF: **Type IIA secretory phospholipase A2 up-regulates cyclooxygenase-2 and amplifies cytokine-mediated prostaglandin production in human rheumatoid synoviocytes.** *J Immunol* 2000, **165**:2790-2797.
9. Feldmann M: **What is the mechanism of action of anti-tumour necrosis factor-alpha antibody in rheumatoid arthritis?** *Int Arch Allergy Immunol* 1996, **111**:362-365.
10. Akira S, Kishimoto T: **IL-6 and NF-IL6 in acute-phase response and viral infection.** *Immunol Rev* 1992, **127**:25-50.
11. Papadakis KA, Targan SR: **Tumor necrosis factor: biology and therapeutic inhibitors.** *Gastroenterology* 2000, **119**:1148-1157.
12. Triggiani M, Granata F, Oriente A, Gentile M, Petraroli A, Balestrieri B, Marone G: **Secretory phospholipases A2 induce cytokine release from blood and synovial fluid monocytes.** *Eur J Immunol* 2002, **32**:67-76.
13. Murakami M, Kuwata H, Amakasu Y, Shimbara S, Nakatani Y, Atsumi G, Kudo I: **Prostaglandin E2 amplifies cytosolic phospholipase A2- and cyclooxygenase-2-dependent delayed prostaglandin E2 generation in mouse osteoblastic cells. Enhancement by secretory phospholipase A2.** *J Biol Chem* 1997, **272**:19891-19897.
14. Schrier DJ, Flory CM, Finkel M, Kuchera SL, Lesch ME, Jacobson PB: **The effects of the phospholipase A2 inhibitor, manoalide, on cartilage degradation, stromelysin expression, and synovial fluid cell count induced by intraarticular injection of human recombinant interleukin-1 alpha in the rabbit.** *Arthritis Rheum* 1996, **39**:1292-1299.
15. Garcia-Pastor P, Randazzo A, Gomez-Paloma L, Alcaraz MJ, Paya M: **Effects of petrosaspongiolide M, a novel phospholipase A2 inhibitor, on acute and chronic inflammation.** *J Pharmacol Exp Ther* 1999, **289**:166-172.
16. Miele L: **Antiflammins. Bioactive peptides derived from uteroglobin.** *Ann N Y Acad Sci* 2000, **923**:128-140.
17. Thwin MM, Gopalakrishnakone P, Kini RM, Armugam A, Jeyaseelan K: **Recombinant antitoxic and antiinflammatory factor from the nonvenomous snake Python reticulatus: phospholipase A2 inhibition and venom neutralizing potential.** *Biochemistry* 2000, **39**:9604-9611.
18. Thwin MM, Satish RL, Chan ST, Gopalakrishnakone P: **Functional site of endogenous phospholipase A2 inhibitor from python serum.** *Eur J Biochem* 2002, **269**:719-727.
19. Thwin MM, Ong WY, Fong CW, Sato K, Kodama K, Farooqui AA, Gopalakrishnakone P: **Secretory phospholipase A2 activity in the normal and kainate injected rat brain, and inhibition by a**

peptide derived from python serum. *Exp Brain Res* 2003, **150**:427-433.
20. Keffer J, Probert L, Cazlaris H, Georgopoulos S, Kaslaris E, Kioussis D, Kollias G: **Transgenic mice expressing human tumour necrosis factor: a predictive genetic model of arthritis.** *EMBO J* 1991, **10**:4025-4031.
21. Wooley PH: **Collagen-induced arthritis in the mouse.** *Methods Enzymol* 1988, **162**:361-373.
22. Douni E, Sfikakis PP, Haralambous S, Fernandes P, Kollias G: **Attenuation of inflammatory polyarthritis in TNF transgenic mice by diacerein: comparative analysis with dexamethasone, methotrexate and anti-TNF protocols.** *Arthritis Res Ther* 2004, **6**:R65-R72.
23. Arsenault AL, Lhotak S, Hunter WL, Banquerigo ML, Brahn E: **Taxol (paclitaxel) involution of articular cartilage destruction in collagen induced arthritis: an ultrastructural demonstration of an increased superficial chondroprotective layer.** *J Rheumatol* 2000, **27**:582-588.
24. Henzgen S, Petrow PK, Thoss K, Brauer R: **Degradation of articular cartilage during the progression of antigen-induced arthritis in mice. A scanning and transmission electron microscopic study.** *Exp Toxicol Pathol* 1996, **48**:255-263.
25. Lapadula G, Nico B, Cantatore FP, La Canna R, Roncali L, Pipitone V: **Early ultrastructural changes of articular cartilage and synovial membrane in experimental vitamin A-induced osteoarthritis.** *J Rheumatol* 1995, **22**:1913-1921.
26. Ghadially FN: *Fine structure of the synovial joints. A text and atlas of the ultrastructure of normal and pathological articular tissues* London: Butterworth; 1983.
27. Redlich K, Hayer S, Maier A, Dunstan CR, Tohidast-Akrad M, Lang S, Turk B, Pietschmann P, Woloszczuk W, Haralambous S, Kollias G, Steiner G, Smolen JS, Schett G: **Tumor necrosis factor alpha-mediated joint destruction is inhibited by targeting osteoclasts with osteoprotegerin.** *Arthritis Rheum* 2002, **46**:785-792.
28. Han Z, Chang L, Yamanishi Y, Karin M, Firestein GS: **Joint damage and inflammation in c-Jun N-terminal kinase 2 knockout mice with passive murine collagen-induced arthritis.** *Arthritis Rheum* 2002, **46**:818-823.
29. Snyder DW, Bach NJ, Dillard RD, Draheim SE, Carlson DG, Fox N, Roehm NW, Armstrong CT, Chang CH, Hartley LW, Johnson LM, Roman CR, Smith AC, Song M, Fleisch JH: **Pharmacology of LY315920/S-5920, [[3-(aminooxoacetyl)-2-ethyl-1- (phenylmethyl)-1H-indol-4-yl]oxy] acetate, a potent and selective secretory phospholipase A2 inhibitor: A new class of anti-inflammatory drugs, SPI.** *J Pharmacol Exp Ther* 1999, **288**:1117-1124.
30. Li P, Schwarz EM: **The TNF-alpha transgenic mouse model of inflammatory arthritis.** *Springer Semin Immunopathol* 2003, **25**:19-33.
31. Nevalainen TJ, Marki F, Kortesuo PT, Grutter MG, Di Marco S, Schmitz A: **Synovial type (group II) phospholipase A2 in cartilage.** *J Rheumatol* 1993, **20**:325-330.
32. Pruzanski W, Bogoch E, Katz A, Wloch M, Stefanski E, Grouix B, Sakotic G, Vadas P: **Induction of release of secretory nonpancreatic phospholipase A2 from human articular chondrocytes.** *J Rheumatol* 1995, **22**:2114-2119.
33. Miyaura C, Inada M, Matsumoto C, Ohshiba T, Uozumi N, Shimizu T, Ito A: **An essential role of cytosolic phospholipase A2alpha in prostaglandin E2-mediated bone resorption associated with inflammation.** *J Exp Med* 2003, **197**:1303-1310.
34. Kudo I, Murakami M: **Diverse functional coupling of prostanoid biosynthetic enzymes in various cell types.** *Adv Exp Med Biol* 1999, **469**:29-35.
35. Balsinde J, Balboa MA, Insel PA, Dennis EA: **Regulation and inhibition of phospholipase A2.** *Annu Rev Pharmacol Toxicol* 1999, **39**:175-189.
36. Vadas P: **Elevated plasma phospholipase A2 levels: correlation with the hemodynamic and pulmonary changes in gram-negative septic shock.** *J Lab Clin Med* 1984, **104**:873-881.
37. Mayer RJ, Marshall LA: **New insights on mammalian phospholipase A2(s); comparison of arachidonoyl-selective and -nonselective enzymes.** *FASEB J* 1993, **7**:339-348.
38. Church WB, Inglis AS, Tseng A, Duell R, Lei PW, Bryant KJ, Scott KF: **A novel approach to the design of inhibitors of human secreted phospholipase A2 based on native peptide inhibition.** *J Biol Chem* 2001, **276**:33156-33164.
39. Lambeau G, Lazdunski M: **Receptors for a growing family of secreted phospholipases A2.** *Trends Pharmacol Sci* 1999, **20**:162-170.
40. Murakami M, Koduri RS, Enomoto A, Shimbara S, Seki M, Yoshihara K, Singer A, Valentin E, Ghomashchi F, Lambeau G, Gelb MH, Kudo I: **Distinct arachidonate-releasing functions of mammalian secreted phospholipase A2s in human embryonic kidney 293 and rat mastocytoma RBL-2H3 cells through heparan sulfate shuttling and external plasma membrane mechanisms.** *J Biol Chem* 2001, **276**:10083-10096.
41. Granata F, Balestrieri B, Petraroli A, Giannattasio G, Marone G, Triggiani M: **Secretory phospholipases A2 as multivalent mediators of inflammatory and allergic disorders.** *Int Arch Allergy Immunol* 2003, **131**:153-163.

Chemistry & Biology, Vol. 11, 1053–1058, August, 2004, ©2004 Elsevier Ltd. All rights reserved. DOI 10.1016/j.chembiol.2004.05.012

Modification of Intracellular Ca^{2+} Dynamics by Laser Inactivation of Inositol 1,4,5-Trisphosphate Receptor Using Membrane-Permeant Probes

Takatoshi Yogo,[1] Kazuya Kikuchi,[1,3] Takanari Inoue,[1] Kenzo Hirose,[2] Masamitsu Iino,[2] and Tetsuo Nagano[1,*]
[1]Graduate School of Pharmaceutical Sciences
[2]Department of Pharmacology
Graduate School of Medicine
The University of Tokyo
7-3-1 Hongo
Bunkyo-ku, Tokyo 113-0033
[3]PRESTO
Japan Science and Technology Corporation
Kawaguchi, Saitama
Japan

Summary

A membrane-permeant malachite green-conjugated IP_3 analog ($MGIP_3$/PM) was synthesized as a probe for small molecule-based CALI (smCALI), and its effect on the Ca^{2+} signaling in intact DT40 chicken B cells was examined. In DT40 B cells treated with the smCALI probe, laser irradiation inhibited IP_3-induced Ca^{2+} oscillations in response to B cell receptor stimulation, demonstrating that IP_3R was acutely inactivated. We then applied smCALI to clarify the mechanism of capacitative Ca^{2+} entry (CCE), in which involvement of IP_3R has been suggested. Despite the inactivation of IP_3R by smCALI, thapsigargin-induced CCE remained unaffected, providing evidence that functional IP_3R is not required for CCE in DT40 cells. These results demonstrate the potency of the smCALI technique for the study of the roles of IP_3R in complex intracellular Ca^{2+} dynamics.

Introduction

Specific inactivation of biomolecules has been one of the most widely used approaches to study the physiological functions of these molecules, and various methods, including the use of pharmacological antagonists, targeted gene disruption, and antibodies, have been used. The activities of most functional biomolecules depend upon the site of expression and the nature of the cellular processes in which they are involved [1–3], so a technique for inactivation of target proteins in a spatiotemporally well controlled manner should be extremely useful. To achieve this purpose, chromophore-assisted laser inactivation (CALI) is an excellent method [4, 5], in which the protein of interest is targeted by an exogenously introduced antibody that has been tagged with a CALI chromophore, usually malachite green, and the chromophore-antibody complex is subsequently irradiated with intense localized laser light. The irradiated chromophore produces radical species that react with the protein to which the antibody is bound, causing its inactivation. Because the radical species are highly reactive and have very short lifetimes, the antibody-recognized proteins are specifically inactivated. The functions of various molecules, which could not have been analyzed by other currently available methods, have been elucidated by inactivation of target proteins at the appropriate site and time using the CALI technique.

Although CALI has proved very powerful, it has some limitations, which are primarily attributable to the use of antibody for the molecular recognition. It is difficult to label antibodies with chromophores at specific amino acid residues, so that the extent of the damage inflicted on the target protein cannot readily be controlled. Moreover, it is necessary to use an invasive method to introduce antibodies into cells, which may jeopardize the physiological functions and long-term viability of the cells. Further, invasive methods (such as trituration, whole-cell clamp, or microinjection) can be applied to only a few cells at a time and are not applicable to tissues.

To circumvent the limitations associated with conventional CALI, we have set out to develop a new method in which synthetic small molecules are used instead of antibody for target recognition (small molecule-based CALI, or smCALI). We designed and synthesized suitable synthetic small molecular probes for biological application of CALI. For the implementation of smCALI, we chose inositol 1,4,5-trisphosphate receptor (IP_3R) as a target protein. IP_3R is a Ca^{2+} channel localized on the endoplasmic reticulum (ER) membrane, and regulates the cytosolic Ca^{2+} concentration, playing an important role in various physiological functions, such as contraction, secretion, fertilization, synaptic plasticity, and gene expression [6, 7]. Thus, spatiotemporally controlled inactivation of IP_3R using smCALI should be useful for studying of the role of the protein in these functions.

We developed a chromophore-labeled IP_3 analog (carboxymalachite green-aminopropyl-1D-*myo*-inositol-1,4,5-trisphosphate, $MGIP_3$) and showed that spatially controlled inactivation of IP_3R could be achieved within a few seconds by $MGIP_3$-mediated smCALI [8–10]. The time required for smCALI is very much shorter than that of antibody-based CALI, which usually requires ~5 min. Furthermore, by focusing a laser beam at the subcellular level in a single PC12 cell, precise control of the area of inactivation could be achieved. In the present study, we derivatized $MGIP_3$ to a membrane-permeant compound for noninvasive delivery into living cells. This membrane-permeant probe can be easily applied to intact cells or cell populations and smCALI experiments can be conducted under physiological conditions. We describe here the successful application of smCALI in intact cells using the membrane-permeant probe, and we show that smCALI provides a powerful tool to analyze complex intracellular Ca^{2+} dynamics.

Results and Discussion

$MGIP_3$/PM Permeates through the Plasma Membrane and Interacts with IP_3R

In previous studies, we designed and synthesized a chromophore-labeled IP_3 analog ($MGIP_3$, Figure 1) and

*Correspondence: tlong@mol.f.u-tokyo.ac.jp

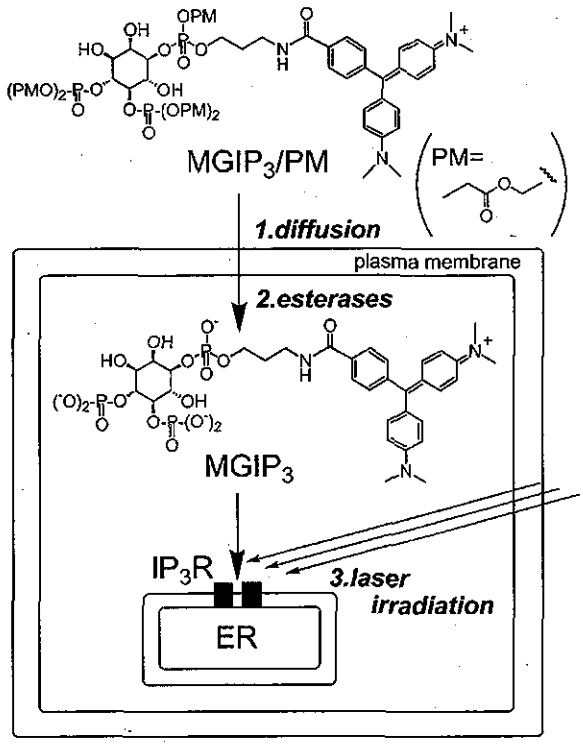

Figure 1. Scheme of smCALI Using a Membrane-Permeant Synthetic Probe, $MGIP_3/PM$

IP_3R, inositol 1,4,5-trisphosphate receptor; ER, endoplasmic reticulum; PM, propionyloxymethyl group.

showed that $MGIP_3$ could act as an agonist of IP_3R and function as an effective probe for smCALI of IP_3R [9, 10]. Permeabilization of the cell membrane or whole-cell patch-clamp was required to introduce $MGIP_3$ into cells, because $MGIP_3$ cannot permeate through the plasma membrane due to its charge and hydrophilicity. Thus, we derivatized $MGIP_3$ to a membrane-permeant compound (carboxymalachite green-aminopropyl-1D-*myo*-inositol-1,4,5-trisphosphate hexakis (propionyloxymethyl) ester, $MGIP_3/PM$, Figure 1) by masking all the anionic phosphate groups with propionyloxymethyl esters. This compound is expected to diffuse into cells, where it should undergo cleavage by the ubiquitous intracellular esterases to generate the hydrolyzed form (i.e., $MGIP_3$), which binds to IP_3R (Figure 1).

We examined whether $MGIP_3/PM$ can indeed permeate through the plasma membrane and interact with IP_3R by using DT40 cells expressing type 2 IP_3R (IP_3R-2). $MGIP_3$ is an agonist of IP_3R and induces Ca^{2+} release via IP_3R in permeablized DT40 cells. Thus, one would expect to observe an increase in $[Ca^{2+}]_i$, if extracellularly applied $MGIP_3/PM$ dose permeate through the plasma membrane and subsequently undergo hydrolysis to yield $MGIP_3$. When $MGIP_3/PM$ (100 μM) was added to the extracellular solution of DT40 cells, it induced an increase in $[Ca^{2-}]_i$, indicating that $MGIP_3/PM$ did enter the cells and interact with IP_3R (Figure 2A, black trace; Figure 2B). On the other hand, extracellularly added $MGIP_3$ (100 μM) or vehicle (0.1% DMSO) induced no detectable $[Ca^{2-}]_i$ increase (Figure 2A, green and blue

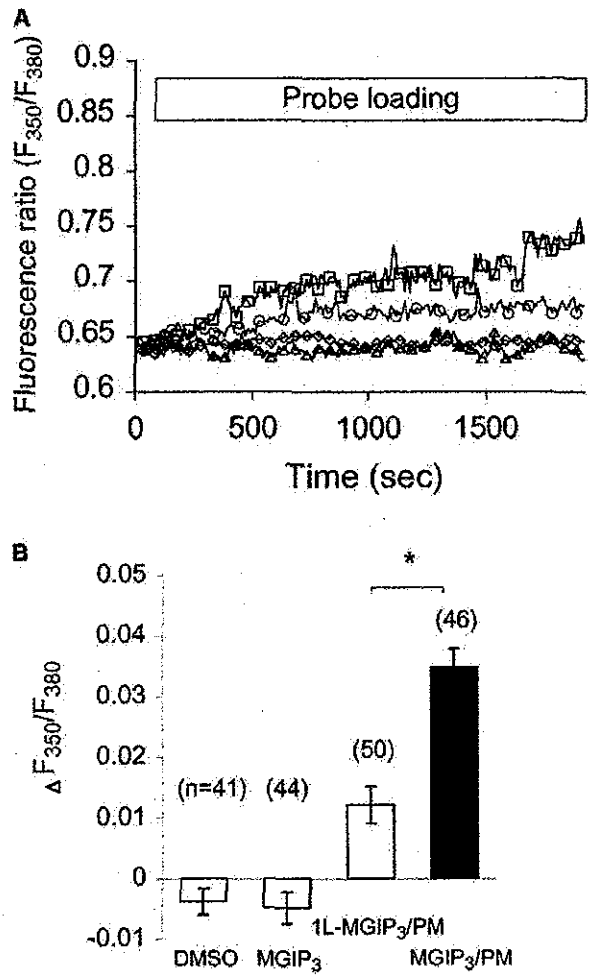

Figure 2. $[Ca^{2+}]_i$ Increase Induced by 100 μM $MGIP_3/PM$ in Intact DT40 Cells

(A) $[Ca^{2+}]_i$ increase induced by 100 μM $MGIP_3/PM$, 100 μM 1L-$MGIP_3/PM$, 100 μM $MGIP_3$, and vehicle (0.1% DMSO). Test compounds were added to an extracellular solution of Fura-2-loaded DT40 cells as indicated by the box. All traces show Ca^{2+} responses in single DT40 cells. 100 μM $MGIP_3/PM$ (black square) induced a much greater $[Ca^{2+}]_i$ increase than 100 μM 1L-$MGIP_3/PM$ (red circle). 100 μM $MGIP_3$ (green diamond) or vehicle (blue triangle) induced no detectable $[Ca^{2+}]_i$ increase.

(B) $[Ca^{2+}]_i$ increase induced by 100 μM $MGIP_3/PM$ and 100 μM 1L-$MGIP_3/PM$. 100 μM $MGIP_3/PM$ induced a significantly larger increase of the fluorescence ratio than 100 μM 1L-$MGIP_3/PM$ within 1800 s after extracellular addition of each compound (*$p < 0.0001$). These data were acquired in two independent experiments. The number of analyzed cells is indicated on top of each column. Results are the mean ± SEM.

traces; Figure 2B), indicating that masking of the phosphate groups is essential for membrane permeation. As a control experiment, we used the optical isomer of $MGIP_3/PM$ (1L-$MGIP_3/PM$), which has the same photochemical nature as that of $MGIP_3/PM$, though its hydrolyzed form (i.e., 1L-$MGIP_3$) has a much weaker agonistic effect on IP_3R [9, 10]. 1L-$MGIP_3/PM$ (100 μM) was much less effective in increasing $[Ca^{2+}]_i$ than $MGIP_3/PM$ and a significant difference in their Ca^{2+} releasing activity was observed (Figures 2A, red versus black traces; Figure 2B, $p < 0.0001$). In all experiments, cells

showed the same responses to B cell receptor stimulation. We also examined the concentration of $MGIP_3$ in the cell by HPLC. After uptake of $MGIP_3$/PM from the exracellular solution by DT40 cells, cells were washed and disrupted by sonication; then the intracellular solution was analyzed by HPLC. The result suggested that the concentration of $MGIP_3$ was at most 10 μM in the cell when $MGIP_3$/PM was extracellularly applied at a concentration of 100 μM (data not shown). This range of $MGIP_3$ concentration is the same as that used in the previous study [10], in which the specificity of CALI was established. Furthermore, DT40 cells lacking all three type of IP_3R [11] exhibited no detectable $[Ca^{2+}]_i$ increase in response to extracellular addition of 100 μM $MGIP_3$/PM (data not shown). These results indicate that $MGIP_3$/PM can permeate through the plasma membrane and interact with IP_3R after intracellular hydrolysis.

Although $MGIP_3$/PM has an inherent agonistic effect, at low concentrations $MGIP_3$/PM induced no detectable $[Ca^{2+}]_i$ increase. Indeed, there was no significant difference between the increase of fluorescence ratio induced by 4 μM $MGIP_3$/PM and that by 4 μM 1L-$MGIP_3$/PM (-0.009 ± 0.006 and -0.013 ± 0.006, respectively, $p = 0.6825$). Thus, we used 4 μM $MGIP_3$/PM for smCALI so that the agonistic effect of the ester could be neglected.

$MGIP_3$/PM-Mediated smCALI Inactivates IP_3R in Intact DT40 Cells

Stimulating the B cell antigen receptor (BCR) induces production of IP_3 via phospholipase C (PLC)-γ2, followed by repetitive cyclic increases in $[Ca^{2+}]_i$ (Ca^{2+} oscillation) in DT40 cells [12]. In the previous study, we showed that $MGIP_3$-mediated smCALI inhibited IP_3-induced Ca^{2} release in permeabilized DT40 cells [10]. We then examined whether laser beam irradiation focused onto intact single DT40 cells loaded with $MGIP_3$/PM induces protein inactivation, by measuring the IP_3-induced Ca^{2+} oscillation. Fura-2-loaded DT40 cells were loaded with 4 μM $MGIP_3$/PM for 60 min, and then we routinely allowed an incubation period of ≥30 min to ensure complete hydrolysis of $MGIP_3$/PM after wash-out of excess ester. $MGIP_3$ in the cell is expected to be stable because it has been shown that inositol 1,4,5- trisphosphate derivatives modified at 1-phosphate are not substrates for 5-phosphatase or 3-kinase [13]. Subsequently, several $MGIP_3$/PM-loaded cells were successively irradiated with the laser for 60 s each (Figure 3A), followed by induction of Ca^{2+} oscillation by BCR stimulation with anti-BCR antibody M4 (1 μg ml^{-1}) [12]. Ca^{2+} oscillation was strongly inhibited in irradiated cells (Figure 3B). The average number of Ca^{2+} oscillations within 500 s after BCR stimulation was decreased by 50% in irradiated cells compared with nonirradiated cells (Figures 3C and 3D, $p < 0.0001$). $MGIP_3$/PM-mediated smCALI also decreased the average peak amplitude of Ca^{2+} oscillations: 2.04 ± 0.10 in irradiated cells and 2.41 ± 0.07 in nonirradiated cells ($p < 0.005$).

Laser irradiation alone in the absence of $MGIP_3$/PM had no significant effect on the average number of Ca^{2+} oscillations (Figure 3D, $p > 0.82$). We then examined whether or not the laser-induced inhibitory effect on Ca^{2+} oscillation is also observed in 1L-$MGIP_3$/PM-loaded cells. No effect of laser irradiation on the average number of Ca^{2+} oscillations was observed in cells loaded with 4 μM 1L-$MGIP_3$/PM (Figure 3D, $p > 0.36$). These results indicate that there is no nonspecific laser damage to IP_3R, and that the inhibition of Ca^{2+} oscillation was the result of IP_3R inactivation by $MGIP_3$/PM-mediated smCALI.

$MGIP_3$-mediated smCALI has been shown to inhibit IP_3-induced Ca^{2+} release [10]. Therefore, it seems likely that Ca^{2+} oscillation was inhibited as a result of the inhibition of IP_3-induced Ca^{2+} release. Ca^{2+} oscillation is a genuine physiological phenomenon, and it is not appropriate to analyze it by using methods that disrupt the intact cell structure, for example, using detergents or microinjection. SmCALI provides the opportunity to analyze Ca^{2+} signaling under physiological conditions.

It was not clear quantitatively to what extent the IP_3R was inactivated by our procedure, but the oscillation frequency, an important factor of Ca^{2+} signaling, was greatly reduced, except for a few initial spikes, as a result of IP_3R inactivation.

Absence of Involvement of IP_3R in Capacitative Calcium Entry

After release of Ca^{2+} from intracellular stores via IP_3R, Ca^{2+} entry across the plasma membrane follows in many cell types [14]. This Ca^{2+} signaling is called capacitative Ca^{2+} entry (CCE). CCE is thought to form an important component of Ca^{2+} signaling. Although IP_3R has been implicated in CCE, the molecular mechanism of CCE remains elusive [15–17]. To study whether IP_3R is involved in CCE, CCE was examined in cells in which IP_3R had been inactivated by smCALI. Inactivation of IP_3R in DT40 cells expressing IP_3R-2 by smCALI was carried under the same conditions as the above experiments. Ca^{2+} stores were then depleted by applying 1 μM thapsigargin (TG), an inhibitor of sarco/endoplasmic reticulum Ca^{2+}-ATPase (SERCA) [18], in the absence of extracellular Ca^{2+}. Subsequent addition of 2 mM Ca^{2+} evoked an increase in $[Ca^{2+}]_i$ due to CCE (Figure 4A). The amplitude of the CCE-mediated increase in $[Ca^{2+}]_i$ was not significantly different between irradiated and nonirradiated cells ($p > 0.86$, Figure 4B), suggesting that the activation of IP_3R is not essential for TG-induced CCE in DT40 cells under these experimental conditions.

It has been suggested that CCE is regulated by the IP_3R [15]. However, it has been difficult to acutely and specifically inactivate IP_3R. Most of the conventional antagonists of IP_3R have direct inhibitory effects on CCE [17, 19]. Targeted disruption of the IP_3R genes is a powerful method, but may not be free from possible long-term compensatory reactions. Recent findings using mutant DT40 cells, in which all subtypes of IP_3R were deleted, strongly suggested that IP_3R is not involved in CCE, because the cells showed typical CCE or I_{crac} (calcium release-activated calcium current) identical to that observed in wild-type cells [11, 16, 20, 21]. However, it was suggested that ryanodine receptors would work as a compensatory mechanism in the mutant DT40 cells [22]. Taking the above circumstances into consideration, smCALI appears to be an excellent method to analyze the functions of IP_3R in CCEs, because acute

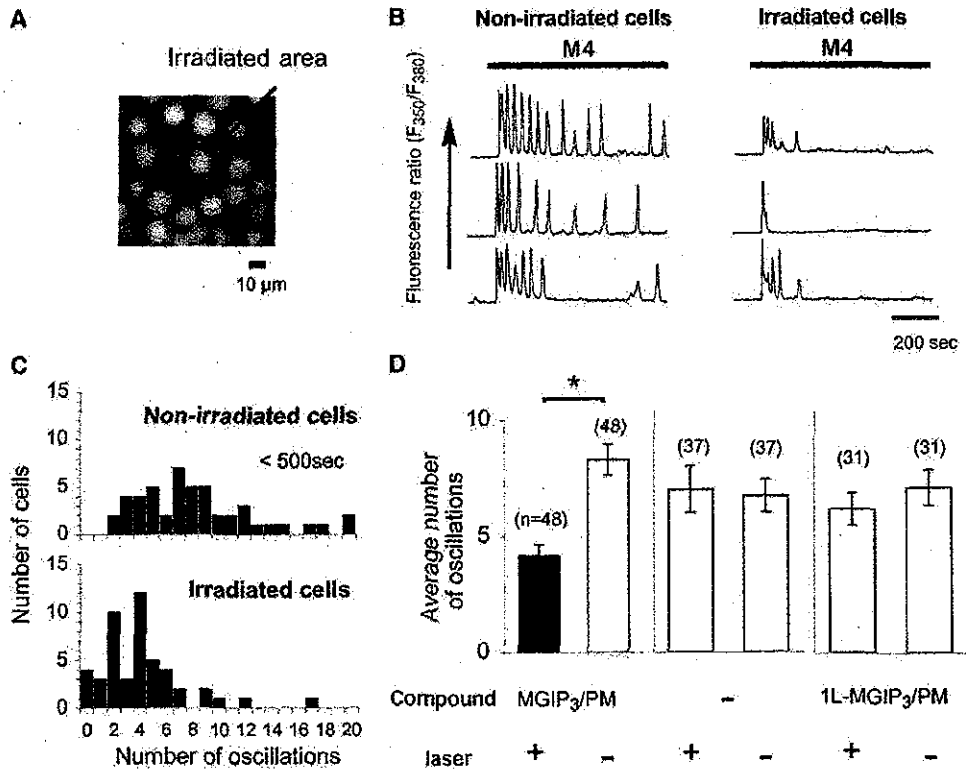

Figure 3. Inhibitory Effect of $MGIP_3$/PM-Mediated smCALI on Ca^{2+} Oscillations in Intact DT40 Cells

(A) Fluorescence image of DT40 cells excited at 350 nm after loading Fura-2AM. The red circle indicates the laser spot for irradiation.

(B) Ca^{2+} responses upon ligation of BCR with *anti-BCR antibody* (1 μg ml^{-1}) after smCALI with 4 μM $MGIP_3$/PM. Traces show several representative responses in irradiated or nonirradiated cells. Antibody was applied as indicated by horizontal bars above the traces.

(C) Histogram showing the number of Ca^{2+} oscillations within 500 s of BCR stimulation in irradiated or nonirradiated cells (48 cells in each condition).

(D) Average number of Ca^{2+} oscillations in response to BCR stimulation after the indicated treatment. A significant difference was found between the average numbers of Ca^{2+} oscillations under irradiated and nonirradiated conditions with $MGIP_3$/PM (*$p < 0.0001$). The number of analyzed cells is indicated on top of each column. These data were acquired in six independent experiments. Results are the mean ± SEM.

inactivation of IP_3R can be carried out under physiological conditions. Other studies have also shown that acute inhibition of IP_3R by heparin (a potent IP_3R angagonist) failed to inhibit I_{crac} [20, 21, 23]. Our results provided evidence that IP_3R is not involved in CCE in DT40 cells. Further application of smCALI should clarify the function of IP_3R in CCE in other cell types.

In the present study we showed that *smCALI can* overcome the main limitation of the conventional CALI technique, in which invasive methods have to be used to introduce antibodies into cells. Indeed, we have succeeded in examining the effect of smCALI on Ca^{2+} oscillations. The role of IP_3R in CCE could be analyzed by smCALI without any long-term compensatory effect. Spatiotemporally controlled genetic modification (conditional knockout) [24] has emerged as a powerful molecular inactivation method. However, it requires a much longer time for molecular inactivation than smCALI. Thus, smCALI provides a unique method to analyze Ca^{2+} signaling under physiological conditions in various cell types. Another feature of $MGIP_3$-mediated smCALI is the catalytic inactivation mechanism [10], i.e., the small-molecular probe ($MGIP_3$) may rapidly associate with and rapidly dissociate from its target (IP_3Rs), and repetitive excitation of malachite green causes cumulative inactivation of IP_3Rs. Due to the catalytic nature of the inactivation, even a low probe concentration may cause sufficient inactivation. Indeed, we showed that 4 μM $MGIP_3$/PM caused sufficient inactivation of IP_3Rs without any agonistic effect. Thus, the smCALI technique provides high spatiotemporal resolution in molecular inactivation, and should be applicable to studies of various physiological functions, especially in polarized cells such as neurons.

Significance

Biological application of conventional CALI has been hampered mainly by the necessity to use invasive *methods to introduce* antibodies into the cells for target recognition. In the present study, we successfully carried out smCALI in intact cells by using membrane-permeant synthetic small molecules. Some variations of small molecule-based CALI have been developed. For example, arsenic chromophore derivatives designed to specifically bind to a tetracysteine tag attached to a target protein induce target inactivation under light *illumination* (FlAsH-FALI) [25, 26]. Although

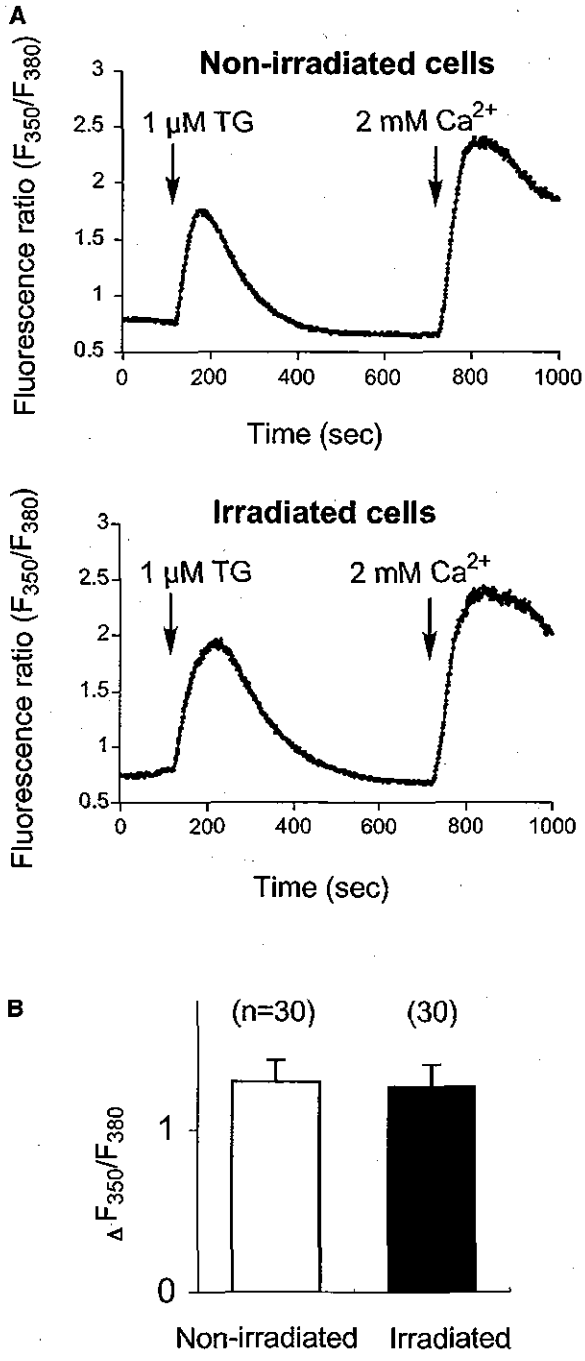

Figure 4. The Effect of $MGIP_3$/PM-Mediated smCALI on Thapsigargin-Induced Capacitative Calcium Entry in DT40 Cells

(A) Intracellular Ca^{2+} release and Ca^{2+} influx were measured in TG-stimulated irradiated and nonirradiated cells. After washing of the cells with Ca^{2+}-free solution, 1 μM TG was used to deplete the Ca^{2+} store, followed by addition of 2 mM Ca^{2+}.

(B) Increase of fluorescence ratio induced by addition of 2 mM Ca^{2+} after TG treatment of irradiated and nonirradiated cells. No significant difference was found between irradiated and nonirradiated cells ($p > 0.86$). The number of analyzed cells is indicated on top of each column. These data were acquired in three independent experiments. Results are the mean ± SEM.

this method is powerful, toxicity and nonspecific damage [27] can be problematic. In our smCALI strategy, we showed that there is no apparent nonspecific damage to IP_3R, presumably due to the catalytic nature of the inactivation and high efficiency. We demonstrated that intracellular Ca^{2+} dynamics can be modified by smCALI of IP_3R under physiological conditions. Since IP_3R is an important regulator of intracellular Ca^{2+} dynamics, spatiotemporally specific inactivation of IP_3R by smCALI using $MGIP_3$/PM may provide a useful method for clarifying the complex Ca^{2+} signaling mechanisms in intact living cells. smCALI should also be applicable to targets other than IP_3R, if appropriate malachite green-conjugated ligands are synthesized.

Experimental Procedures

Synthesis of $MGIP_3$/PM

$MGIP_3$ was synthesized as reported previously [8]. To synthesize $MGIP_3$/PM, $MGIP_3$ (1.0 eq.) was mixed vigorously with CH_3CN and *N, N*-diisopropylethylamine (DIEA) (2.0 eq.). The mixture was then dried under vacuum. This procedure was repeated at least three times until a homogenous solution was obtained after adding CH_3CN/DIEA. After a final round of drying, the green solid was suspended in CH_3CN and DIEA (5.0 eq.). Bromomethyl propionate (5.0 eq.) [28] was added to this solution. The mixture was stirred for 24 hr, then further bromomethyl propionate (2.5 eq.) and DIEA (2.5 eq.) were added and the reaction was continued for another 24 hr. The solvent and excess reagents were evaporated under vacuum. The remaining mixture was purified by C_{18} reversed-phase HPLC. ^{1}H-NMR (CD_3OD): δ1.02 (m, 15H), 1.80 (m, 2H), 1.93 (br, 2H), 2.32 (m, 10H), 3.30~5.50 (m, 10H), 3.60 (s, 12H), 5.61 (br, 10H), 7.30 (m, 2H), 7.58 (m, 4H), 7.78 (m, 6H). 1L-$MGIP_3$/PM was also synthesized in the same manner.

Cell Culture

DT40 chicken B lymphoma cells were cultured in RPMI1640 supplemented with 10% fetal calf serum (FCS), 1% chicken serum, penicillin (100 U/ml), streptomycin (100 U/ml), and 2 mM glutamine. In some experiments, genetically engineered DT40 cells that express only type 2 IP_3R or that lack all three type of IP_3R were used [11, 12].

Ca^{2+} Imaging

Cells were attached to poly-L-lysine and collagen-coated coverslips and loaded with 1 μM Fura-2AM (Molecular Probes) for 30 min in a physiological salt solution (PSS: 150 mM NaCl, 4 mM KCl, 2 mM $CaCl_2$, 1 mM $MgCl_2$, 5 mM HEPES, 5.6 mM glucose, pH 7.4) containing 0.1% bovine serum albumin (BSA). An Olympus IX71 inverted microscope, equipped with a cooled CCD camera (Photometrics) and a polychromatic illumination system (T.I.L.L. Photonics) was used to capture the fluorescence images generated by alternate excitations at 350 and 380 nm every 1 or 10 s. Intracellular Ca^{2+} concentration was measured as the ratio of the fluorescence intensity between the pair of frames (F_{350}/F_{380}). The test compounds were predissolved in PSS (containing 0.1% DMSO).

Laser Irradiation for smCALI

A nitrogen-driven pulsed dye laser (wavelength 635 nm, pulse width <4 ns, and pulse energy ~30 μJ at 20 Hz; Laser Science Inc.;VSL-337ND-S and DUO-220) was spatially filtered using a pair of objective lenses. A circular beam with a required spot size was introduced into a water-immersion objective (60×, NA 0.90, Olympus) attached to the inverted fluorescence microscope. The laser beam was focused onto a single DT40 cell. The diameters of the laser spot and a single DT40 cell were 20 and ~15 μm, respectively. The laser pulse energy at the focal plane was ~7 μJ. Laser irradiation was carried out as follows. The probe was added to the extracellular solution of Fura-2-loaded DT40 cells, and after 60 min, the excess ester was washed away with PSS. After ≥30 min, several cells were successively irradiated for 60 s. For the analysis of nonirradiated

cells surrounding irradiated cells, we randomly selected cells within a frame.

Statistical Analyses

Statistical analysis was performed using Student's unpaired t-test.

Acknowledgments

This work was supported in part by the Ministry of Education, Culture, Sports, Science, and Technology of Japan (grants 11794026, 12470475, and 12557217 to T.N., 13558078, 14045210, and 15681012 to K.K.), by the Mitsubishi Foundation, and by the Research Foundation for Opt-Science and Technology.

Received: January 18, 2004
Revised: May 6, 2004
Accepted: May 11, 2004
Published: August 20, 2004

References

1. Schmucker, D., Su, A.L., Beermann, A., Jäckle, H., and Jay, D.G. (1994). Chromophore-assisted laser inactivation of patched protein switches cell fate in the larval visual-system of *Drosophila*. Proc. Natl. Acad. Sci. USA *91*, 2664–2668.
2. Vernos, I., Raats, J., Hirano, T., Heasman, J., Karsenti, E., and Wylie, C. (1995). Xklp1, a chromosomal *Xenopus* kinesin-like protein essential for spindle organization and chromosome positioning. Cell *81*, 117–127.
3. Kiselyov, K., Xu, X., Mozhayeva, G., Kuo, T., Pessah, I., Mignery, G., Zhu, X., Birnbaumer, L., and Muallem, S. (1998). Functional interaction between $InsP_3$ receptors and store-operated Htrp3 channels. Nature *396*, 478–482.
4. Jay, D.G. (1988). Selective destruction of protein function by chromophore-assisted laser inactivation. Proc. Natl. Acad. Sci. USA *85*, 5454–5458.
5. Jay, D.G., and Sakurai, T. (1999). Chromophore-assisted laser inactivation (CALI) to elucidate cellular mechanisms of cancer. Biochim. Biophys. Acta *1424*, M39–M48.
6. Berridge, M.J. (1993). Inositol trisphosphate and calcium signaling. Nature *361*, 315–325.
7. Berridge, M.J., Bootman, M.D., and Roderick, H.L. (2003). Calcium signalling: dynamics, homeostasis and remodelling. Nat. Rev. Mol. Cell Biol. *4*, 517–529.
8. Inoue, T., Kikuchi, K., Hirose, K., Iino, M., and Nagano, T. (1999). Synthesis and evaluation of 1-position-modified inositol 1,4,5-trisphosphate analogs. Bioorg. Med. Chem. Lett. *9*, 1697–1702.
9. Inoue, T., Kikuchi, K., Hirose, K., Iino, M., and Nagano, T. (2001). Small molecule-based laser inactivation of inositol 1,4,5-trisphosphate receptor. Chem. Biol. *8*, 9–15.
10. Inoue, T., Kikuchi, K., Hirose, K., Iino, M., and Nagano, T. (2003). Spatiotemporal laser inactivation of inositol 1,4,5-trisphosphate receptors using synthetic small-molecule probes. Chem. Biol. *10*, 503–509.
11. Sugawara, H., Kurosaki, M., Takata, M., and Kurosaki, T. (1997). Genetic evidence for involvement of type 1, type 2 and type 3 inositol 1,4,5-trisphosphate receptors in signal transduction through the B-cell antigen receptor. EMBO J. *16*, 3078–3088.
12. Miyakawa, T., Maeda, A., Yamazawa, T., Hirose, K., Kurosaki, T., and Iino, M. (1999). Encoding of Ca^{2+} signals by differential expression of IP_3 receptor subtypes. EMBO J. *18*, 1303–1308.
13. Prestwich, G.D., Marecek, J.F., Mourey, R.J., Theibert, A.B., Ferris, C.D., Danoff, S.K., and Snyder, S.H. (1991). Tethered IP_3. Synthesis and biochemical applications of the 1-O-(3-aminopropyl) ester of inositol 1,4,5-trisphosphate. J. Am. Chem. Soc. *113*, 1822–1825.
14. Venkatachalam, K., van Rossum, D.B., Patterson, R.L., Ma, H.T., and Gill, D.L. (2002). The cellular and molecular basis of store-operated calcium entry. Nat. Cell Biol. *4*, E263–E272.
15. Ma, H.T., Patterson, R.L., van Rossum, D.B., Birnbaumer, L., Mikoshiba, K., and Gill, D.L. (2000). Requirement of the inositol trisphosphate receptor for activation of store-operated Ca^{2+} channels. Science *287*, 1647–1651.
16. Ma, H.T., Venkatachalam, K., Li, H.S., Montell, C., Kurosaki, T., Patterson, R.L., and Gill, D.L. (2001). Assessment of the role of the inositol 1,4,5-trisphosphate receptor in the activation of transient receptor potential channels and store-operated Ca^{2+} entry channels. J. Biol. Chem. *276*, 18888–18896.
17. Bootman, M.D., Collins, T.J., Mackenzie, L., Roderick, H.L., Berridge, M.J., and Peppiatt, C.M. (2002). 2-aminoethoxydiphenyl borate (2-APB) is a reliable blocker of store-operated Ca^{2+} entry but an inconsistent inhibitor of $InsP_3$-induced Ca^{2+} release. FASEB J. *16*, 1145–1150.
18. Thastrup, O., Cullen, P.J., Drobak, B.K., Hanley, M.R., and Dawson, A.P. (1990). Thapsigargin, a tumor promoter, discharges intracellular Ca^{2+} stores by specific-inhibition of the endoplasmic-reticulum Ca^{2+}-ATPase. Proc. Natl. Acad. Sci. USA *87*, 2466–2470.
19. Bultynck, G., Sienaert, I., Parys, J.B., Callewaert, G., De Smedt, H., Boens, N., Dehaen, W., and Missiaen, L. (2003). Pharmacology of inositol trisphosphate receptors. Pflugers Arch. *445*, 629–642.
20. Broad, L.M., Braun, F.J., Lievremont, J.P., Bird, G.S.J., Kurosaki, T., and Putney, J.W. (2001). Role of the phospholipase C-inositol 1,4,5-trisphosphate pathway in calcium release-activated calcium current and capacitative calcium entry. J. Biol. Chem. *276*, 15945–15952.
21. Prakriya, M., and Lewis, R.S. (2001). Potentiation and inhibition of Ca^{2+} release-activated Ca^{2+} channels by 2-aminoethyldiphenyl borate (2-APB) occurs independently of IP_3 receptors. J. Physiol. (London) *536*, 3–19.
22. Kiselyov, K., Shin, D.M., Shcheynikov, N., Kurosaki, T., and Muallem, S. (2001). Regulation of Ca^{2+}-release-activated Ca^{2+} current (I_{crac}) by ryanodine receptors in inositol 1,4,5-trisphosphate-receptor- deficient DT40 cells. Biochem. J. *360*, 17–22.
23. Fierro, L., and Parekh, A.B. (1999). On the characterisation of the mechanism underlying passive activation of the Ca^{2+} release-activated Ca^{2+} current I_{CRAC} in rat basophilic leukaemia cells. J. Physiol. (London) *520*, 407–416.
24. Tsien, J.Z., Chen, D.F., Gerber, D., Tom, C., Mercer, E.H., Anderson, D.J., Mayford, M., Kandel, E.R., and Tonegawa, S. (1996). Subregion- and cell type-restricted gene knockout in mouse brain. Cell *87*, 1317–1326.
25. Marek, K.W., and Davis, G.W. (2002). Transgenically encoded protein photoinactivation (FlAsH-FALI): acute inactivation of synaptotagmin I. Neuron *36*, 805–813.
26. Poskanzer, K.E., Marek, K.W., Sweeney, S.T., and Davis, G.W. (2003). Synaptotagmin I is necessary for compensatory synaptic vesicle endocytosis in vivo. Nature *426*, 559–563.
27. Tour, O., Meijer, R.M., Zacharias, D.A., Adams, S.R., and Tsien, R.Y. (2003). Genetically targeted chromophore-assisted light inactivation. Nat. Biotechnol. *21*, 1505–1508.
28. Li, W.H., Schultz, C., Llopis, J., and Tsien, R.Y. (1997). Membrane-permeant esters of inositol polyphosphates, chemical syntheses and biological applications. Tetrahedron *53*, 12017–12040.

J|A|C|S
COMMUNICATIONS

Published on Web 12/24/2004

Design and Synthesis of Zinc-Selective Chelators for Extracellular Applications

Eri Kawabata,† Kazuya Kikuchi,†,‡ Yasuteru Urano,† Hirotatsu Kojima,† Akira Odani,§ and Tetsuo Nagano*,†

Graduate School of Pharmaceutical Sciences, The University of Tokyo, 7-3-1 Hongo, Bunkyo-ku,Tokyo 113-0033, Japan, Presto, JST Corporation, Kawaguchi, Saitama, Japan, and Department of Chemistry, Graduate School of Science, Nagoya University, Nagoya, Aichi, Japan

Received September 2, 2004; E-mail: tlong@mol.f.u-tokyo.ac.jp

Zinc (Zn^{2+}) is found in every cell in the human body and is mostly tightly bound to proteins as a key component of numerous enzymes and transcription factors.[1,2] Chelatable Zn^{2+} co-localizes with glutamate in the synaptic vesicles of certain glutamatergic vesicles in the mammalian brain, including the hippocampus, amygdala, and neocortex.[3] Free Zn^{2+} exists at a concentration of a few millimolar in the vesicles of presynaptic neurons and is released during synaptic activity or depolarization, modulating the function of certain ion channels and receptors.[4-7] Many reports describe the significance of Zn^{2+} in biological systems,[8-13] but its mechanisms of action are poorly understood.

Although various chemical tools for measuring Zn^{2+} in biological samples, such as fluorescence probes for Zn^{2+}, have been developed,[14-23] better Zn^{2+}-selective chelators are still needed. Research on Zn^{2+} signals in the brain has traditionally employed several chelators, though they have various shortcomings for biological applications. Use of *N,N,N′,N′*-tetrakis(2-pyridylmethyl)-ethylenediamine (TPEN), a classical membrane-permeable Zn^{2+} chelator, does not allow selective manipulation of extracellular or intracellular Zn^{2+}. On the other hand, calcium ethylenediaminetetraacetic acid (CaEDTA), an extracellular (membrane-impermeable) Zn^{2+} chelator, has the disadvantage of slow kinetics of Zn^{2+} binding. Concentrations of CaEDTA that are sufficient to chelate synaptic Zn^{2+} at equilibrium do not effectively chelate Zn^{2+} within the period of tens to hundreds of microseconds that it takes Zn^{2+} to cross the synapse and interact with various postsynaptic sites.[24] In contrast, a higher concentration of CaEDTA markedly reduces the Zn^{2+} and Ca^{2+} signals.[25] This phenomenon makes it difficult to interpret the action mechanism of Zn^{2+} under physiological conditions, where change of Ca^{2+} concentration can also induce various responses. Especially in electrophysiological studies of ion channels and neuronal activities, reduction of extracellular Ca^{2+} can result in neurological side effects. The development of new, more rapid Zn^{2+} chelators which have low affinity for Ca^{2+} is required for the clarification of the mechanism of synaptic release of Zn^{2+}. We report here the design, synthesis, and properties of new Zn^{2+} chelators, and we describe biological application in hippocampal slices.

We designed (4-{[2-(bis-pyridin-2-ylmethylamino)ethylamino]-methyl}phenyl)methanesulfonic acid, sodium salt (DPESA), and [4-({[2-(bis-pyridin-2-ylmethylamino)ethyl]pyridin-2-ylmethylamino}-methyl)phenyl]methanesulfonic acid, sodium salt (TPESA) utilizing TPEN structure for high Zn^{2+} selectivity and a sulfonic acid moiety for hydrophilicity (Figure 1). The acid dissociation constants and metal chelate stability constants were determined by potentiometric methods (Table 1 and Table S1, Supporting Information). The log K values of DPESA and TPESA for Zn^{2+} are 11.8 and 12.3, respectively, showing that these two compounds have high affinity for Zn^{2+}. The log K values for Ca^{2+} are 4.20 and 2.47, and those for Mg^{2+} are 3.97 and 2.66, respectively, indicating low affinity for these metal ions.

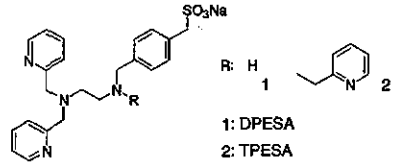

Figure 1. Structures of new zinc-selective chelators.

Table 1. Stability Constants of Chelators

	log K			
M^{n+}	DPESA[a]	TPESA[a]	TPEN[b]	EDTA[b]
Ca^{2+}	4.20 ± 0.11	2.47 ± 0.10	4.40	10.7
Mg^{2+}	3.97 ± 0.10	2.66 ± 0.10	1.70	8.64
Zn^{2+}	11.8 ± 0.01	12.3 ± 0.03	15.4	16.3

[a] Stability constants of DPESA and TPESA were determined at 25 °C, I = 0.1. The determined value ± SD is given. [b] From the SCDatabase (IUPAC and Academic Software): 25 °C, I = 0.1.

To compare the relative association rate constants of the new chelators for Zn^{2+} with those of traditional chelators, competition analysis was performed between Zn^{2+}-fluorescence probe complex and Zn^{2+}-selective chelators (Figure S3, Supporting Information). ZnAF-2[14a] was used as a fluorescence probe for Zn^{2+}; its log K_{obs} value (K_{obs} is the apparent association constant at pH 7.4, I = 0.10 M $NaNO_3$) has been reported as 8.57. The fluorescence intensity of ZnAF-2 (1.0 μM) linearly increased up to a 1:1 [ZnAF-2]/[Zn^{2+}] ratio, and the maximum fluorescence was obtained with 1.0 μM Zn^{2+} addition. Then 10 μM chelator was added and the time course of fluorescence decrease was compared among DPESA, TPESA, TPEN, and CaEDTA. The addition of 10 μM TPESA rapidly decreased the fluorescence with a half-life of 18.6 s, which is comparable to that of TPEN (12.2 s). This result suggested that TPESA can reduce the concentration of synaptically released Zn^{2+} rapidly, without changing the extracellular Ca^{2+} concentration. On the other hand, DPESA reduced the fluorescence with a half-life of 67.0 s, which is similar to the value of 65.4 s obtained for CaEDTA. Considering that DPESA may have the same affinity for Zn^{2+} as ZnAF-2, whereas the other chelators have higher affinities (Table 1), the above result suggests rapid Zn^{2+} chelation.

To examine the membrane permeability of the new chelators, we applied them to hippocampal slices (Figure S4, Supporting Information). Acute rat hippocampal slices were incubated with 10 μM ZnAF-2 DA[14a] for 1.5 h at room temperature for dye loading.

† The University of Tokyo.
‡ Presto, JST Corporation.
§ Nagoya University.

10.1021/ja044697q CCC: $30.25

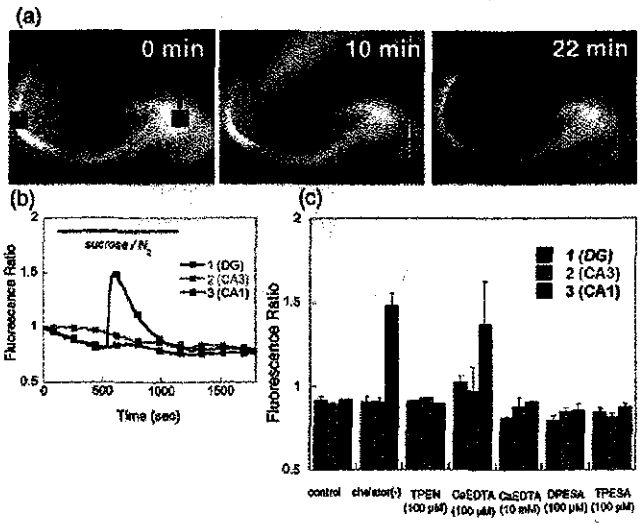

Figure 2. Application of the chelators under ischemic conditions. Dye-loaded slices were exposed to anoxic-aglycemiic ACSF for 17 min (from 2 to 19 min). (a) Fluorescence images at 0, 10, and 22 min after the measurement. The fluorescence ratio in the plot (b) is the ratio of the fluorescence intensity to the initial intensity of the corresponding area in the image at 0 min. (c) Histogram showing the effects of the chelators on the fluorescence change of ZnAF-2 DA-loaded slices under anoxia-aglycemia. Fluorescence ratio in the histogram is the ratio of the fluorescence intensity at 10 min after the start of the measurement to the initial intensity of the corresponding area in the image at 0 min. Each column, except for TPEN, shows the mean ± SE.

ZnAF-2 DA is expected to permeate well through the cell membrane and then to be transformed to ZnAF-2 by esterase in the cytosol, where the dye would be retained for a long time. It interacts with intracellular Zn^{2+} to generate strong fluorescence. The fluorescence was intense in the hilus and the stratum lucidum of the CA3 region, where Zn^{2+} is concentrated in the vesicles.[6] The fluorescence was decreased by extracellular addition of the membrane-permeable chelator TPEN (100 μM) for 30 min, whereas it was scarcely altered by addition of CaEDTA, DPESA, or TPESA. These results support the view that DPESA and TPESA are membrane-impermeable chelators.

It has been suggested that the concentration of intracellular Zn^{2+} at the hippocampal CA1 region transiently increases in response to an ischemic insult, which is content with a relationship between Zn^{2+} and apoptosis.[14b] This increase might be derived from influx of extracellular Zn^{2+} released from the presynaptic terminals, or from the release of Zn^{2+} from intracellular vesicles. To investigate the second possibility, we used DPESA and TPESA (Figure 2).

Acute rat hippocampal slices which had been loaded with ZnAF-2 DA were exposed to anoxic-aglycemic ACSF for 17 min. The fluorescence in the CA1 region increased transiently, but this was not observed when TPEN (100 μM) was added extracellularly (30-min preperfusion with 100 μM TPEN followed by anoxic-aglycemic insult in the presence of 100 μM TPEN). Similarly, the presence of 100 μM DPESA or TPESA inhibited the transient increase in fluorescence, indicating that DPESA and TPESA chelated synaptically released Zn^{2+} quite rapidly and thereby suppressed influx of Zn^{2+} into the cells. These results suggest that Zn^{2+} is released from the presynaptic vesicles in response to an ischemic insult and is taken up intracellularly into the postsynaptic neurons. Notably, 100 μM DPESA or TPESA was sufficient for Zn^{2+} chelation, whereas 100 μM CaEDTA was not. Thus, our newly designed chelators yielded the biologically significant finding that presynaptic Zn^{2+} can be released in the CA1 region. This confirms the utility of these new chelators as extracellular Zn^{2+} chelators for biological applications.

In conclusion, we have developed new membrane-impermeable Zn^{2+}-selective chelators, DPESA and TPESA, with the advantageous characteristics of high Zn^{2+} selectivity and rapid chelation, that can be applied to cell-biological studies to shed additional light on the function of synaptically released Zn^{2+}.

Acknowledgment. This work was supported in part by the Ministry of Education, Culture, Sports, Science and Technology of Japan (Grant Nos. 16370071 to T.N., 15681012 and 16048206 to K.K.). K.K. was also supported by the Sankyo Foundation, the Kanagawa Academy of Science, and the Suzuken Memorial Foundation.

Supporting Information Available: Synthesis, experimental details, and characterization of DPESA and TPESA. This material is available free of charge via the Internet at http://pubs.acs.org.

References

(1) Vallee, B. L.; Falchuk, K. H. *Physiol. Rev.* **1993**, *73*, 79−118.
(2) O'Halloran, T. V. *Science* **1993**, *261*, 715−725.
(3) Frederickson, C. J. *Int. Rev. Neurobiol.* **1989**, *31*, 145−238.
(4) Weiss, J. H.; Sensi, S. L.; Koh, J.-Y. *Trends Pharmacol. Sci.* **2000**, *21*, 395−401.
(5) Molnar, P.; Nadler, J. V. *Brain Res.* **2001**, *910*, 205−207.
(6) Ueno, S.; Tsukamoto, M.; Hirano, T.; Kikuchi, K.; Yamada, M.; Nishikawa, N.; Nagano, T.; Matsuki, N.; Ikegaya, Y. *J. Cell Biol.* **2002**, *158*, 215−220.
(7) Hosie, A. M.; Dunne, E. L.; Harvey, R. J.; Smart, T. G. *Nat. Neurosci.* **2003**, *6*, 362−369.
(8) Bush, A. I.; Pettingel, W. H.; Multhaup, G.; Paradis, M. D.; Vonsattel, J. P.; Gusella, J. F.; Beyreuther, K.; Masters, C. L.; Tanzi, R. E. *Science* **1994**, *265*, 1464−1467.
(9) Koh, J.-Y.; Suh, S. W.; Gwag. B. J.; He, Y. Y.; Hsu, C. Y.; Choi, D. W. *Science* **1996**, *272*, 1013−1016.
(10) Truong-Tran, A. Q.; Ho, L. H.; Chai, F.; Zalewski, P. D. *J. Nutr.* **2000**, *130*, 1459S−1466S.
(11) (a) Suh, S. W.; Chen, J. W.; Motamedi, M.; Bell, B.; Listiak, K.; Pons, N. F.; Danscher, G.; Frederickson, C. J. *Brain Res.* **2000**, *852*, 268−273. (b) Li, Y.; Hough, C. J.; Suh, S. W.; Sarvey, J. M.; Frederickson, C. J. *J. Neurophysiol.* **2001**, *86*, 2597−2604.
(12) Truong-Tran, A. Q.; Carter, J.; Ruffin, R. E.; Zalewski, P. D. *BioMetals* **2001**, *14*, 315−330.
(13) Kay, A. R. *J. Neurosci.* **2003**, *23*, 6847−6855.
(14) (a) Hirano, T.; Kikuchi, K.; Urano, Y.; Higuchi, T.; Nagano, T. *J. Am. Chem. Soc.* **2000**, *122*, 12399−12400. (b) Hirano, T.; Kikuchi, K.; Urano, Y.; Nagano, T. *J. Am. Chem. Soc.* **2002**, *124*, 6555−6562.
(15) Tompson, R. B.; Whetsell, W. O., Jr.; Maliwal, B. P.; Fierke, C. A.; Frederickson, C. J. *J. Neurosci. Methods* **2000**, *96*, 35−45.
(16) (a) Walkup, G. K.; Imperiali, B. *J. Am. Chem. Soc.* **1996**, *118*, 3053−3054. (b) Pearce, D. A.; Jotterand, N.; Carrico, I. S.; Imperiali, B. *J. Am. Chem. Soc.* **2001**, *123*, 5160−5161. (c) Shults, M. D.; Pearce, D. A.; Imperiali, B. *J. Am. Chem. Soc.* **2003**, *125*, 10591−10597.
(17) (a) Fahrni, C. J.; O'Halloran, T. V. *J. Am. Chem. Soc.* **1999**, *121*, 11448−11458. (b) Taki, M.; Wolford, J. L.; O'Halloran, T. V. *Am. Chem. Soc.* **2004**, *126*, 712−713.
(18) (a) Fahrni, C. J.; Henary, M. M.; VanDerveer D. G. *J. Phys. Chem. A* **2002**, *106*, 7655−7663. (b) Henary, M. M.; Wu, Y.; Fahrni, C. J. *Chem. Eur. J.* **2004**, *10*, 3015−3025.
(19) (a) Walkup, G. K.; Burdette, S. C.; Lippard, S. J.; Tsien, R. Y. *J. Am. Chem. Soc.* **2000**, *122*, 5644−5645. (b) Burdette, S. C.; Walkup, G. K.; Spingler, B.; Tsien, R. Y.; Lippard, S. J. *J. Am. Chem. Soc.* **2001**, *123*, 7831−7841. (c) Burdette, S. C.; Frederickson, C. J.; Lippard, S. J. *J. Am. Chem. Soc.* **2003**, *125*, 1778−1787.
(20) (a) Gee, K. R.; Zhou, Z. L.; Qian, W. J.; Kennedy, R. *J. Am. Chem. Soc.* **2002**, *124*, 776−778. (b) Sensi, S. L.; Ton-That, D.; Weiss, J. H.; Rothe, A.; Gee, K. R. *Cell Calcium* **2003**, *34*, 281−284.
(21) Godwin, H. A.; Berg, J. M. *J. Am. Chem. Soc.* **1996**, *118*, 6514−6515.
(22) Budde, T.; Minta, A.; White, J. A.; Kay, A. R. *Neuroscience* **1997**, *79*, 347−358.
(23) Haugland, R. P. *Handbook of Fluorescent Probes and Research Products*, 8th ed.; Molecular Probes, Inc.: Eugene, OR, 2001; Section 20.7.
(24) Vogt, K.; Mellor, J.; Tong, V.; Nicoll, R. *Neuron* **2000**, *26*, 187−196.
(25) Li, Y.; Hough, C. J.; Frederickson, C. J.; Sarvey, J. M. *J. Neurosci.* **2001**, *21*, 8015−8025.

JA044697Q

Gene Therapy (2005) 12, 203–210

www.nature.com/gt

RESEARCH ARTICLE

Efficient and stable Sendai virus-mediated gene transfer into primate embryonic stem cells with pluripotency preserved

K Sasaki[1,2], M Inoue[3], H Shibata[1], Y Ueda[3], S-i Muramatsu[4], T Okada[1], M Hasegawa[3], K Ozawa[1] and Y Hanazono[1]

[1]*Center for Molecular Medicine, Jichi Medical School, Minamikawachi, Tochigi, Japan;* [2]*Department of Plastic and Reconstructive Surgery, Faculty of Medicine, University of Tokyo, Bunkyo-ku, Tokyo, Japan;* [3]*DNAVEC Corporation, Tsukuba, Ibaraki, Japan; and* [4]*Department of Neurology, Jichi Medical School, Minamikawachi, Tochigi, Japan*

Efficient gene transfer and regulated transgene expression in primate embryonic stem (ES) cells are highly desirable for future applications of the cells. In the present study, we have examined using the nonintegrating Sendai virus (SeV) vector to introduce the green fluorescent protein (GFP) gene into non-human primate cynomolgus ES cells. The GFP gene was vigorously and stably expressed in the cynomolgus ES cells for a year. The cells were able to form fluorescent teratomas when transplanted into immunodeficient mice. They were also able to differentiate into fluorescent embryoid bodies, neurons, and mature blood cells. In addition, the GFP expression levels were reduced dose-dependently by the addition of an anti-RNA virus drug, ribavirin, to the culture. Thus, SeV vector will be a useful tool for efficient gene transfer into primate ES cells and the method of using antiviral drugs should allow further investigation for regulated SeV-mediated gene expression.
Gene Therapy (2005) **12**, 203–210. doi:10.1038/sj.gt.3302409
Published online 14 October 2004

Keywords: *primate embryonic stem cell; Sendai virus vector; gene transfer; green fluorescent protein; pluripotency; ribavirin*

Introduction

Since human embryonic stem (ES) cell lines have the ability to both proliferate indefinitely and differentiate into multiple tissue cells,[1,2] they are expected to have clinical applications as well as to serve as models for basic research and drug development. Although efficient and stable gene transfer into primate ES cells would be useful for such purposes, it has been difficult and only lentiviral vectors have been successful in achieving it.[3–5] We have previously developed Sendai virus (SeV) vectors that replicate in the form of negative-sense single-stranded RNA in the cytoplasm of infected cells and do not go through a DNA phase.[6] SeV vectors can efficiently introduce foreign genes without toxicity into airway epithelial cells,[7] vascular tissue,[8] skeletal muscle,[9] synovial cells,[10] retinal tissue,[11] and hematopoietic progenitor cells.[12] Here we report that the SeV-mediated gene transfer into primate ES cells is very efficient and stable even after the terminal differentiation of the cells. In addition, we show that SeV-mediated transgene expression levels can be reduced by the addition of a ribonucleoside analog, ribavirin, to the culture. Ribavirin is a mutagen and inhibitor of viral RNA polymerase.[13,14] It shows antiviral activity against a variety of RNA viruses and is used to treat infections of hepatitis C virus in combination with interferon-α[15,16] and of lassa fever virus.[17] The method of using antiviral drugs might offer a novel approach for regulated SeV-mediated gene expression in primate ES cells.

Correspondence: Dr Y Hanazono, Center for Molecular Medicine, Jichi Medical School, 3311-1 Yakushiji, Minamikawachi, Tochigi 329-0498, Japan
Received 20 April 2004; accepted 27 August 2004; published online 14 October 2004

Results

SeV-mediated gene transfer into ES cells

In this study, we have used an SeV vector, which is capable of self-replication but incapable of transmitting to other cells.[6] The vector does not encode the fusion (F) protein (Figure 1a), which is essential for viral entry into cells. It can be propagated only in a packaging cell line expressing the F protein. The green fluorescent protein (GFP) gene was introduced after the leader sequence of the vector genome. Cynomolgus ES cells[18] were exposed to the SeV vector for 24 h. Flow cytometric analysis at 2 days after infection showed that 15, 38, and 61% of cells fluoresced at 2, 10, and 50 transducing units (TU) per cell, respectively (Figure 1b). The gene transfer efficiency of about 60% is comparable to or even better than that for lentiviral vectors.[3] We confirmed that the undifferentiated cell fractions remained unchanged after the infection with SeV vector, as assessed by the expression of undifferentiated markers, alkaline phosphatase and SSEA-4 (data not shown). The GFP expression after infection was stable at least for a month. On the other hand, the GFP gene transfer to cynomolgus ES cells with adenovirus- and adeno-associated virus (AAV)-based vectors resulted in much lower expression levels (<20% by flow cytometry) and the levels declined to zero within a week after infection (Figure 1c).

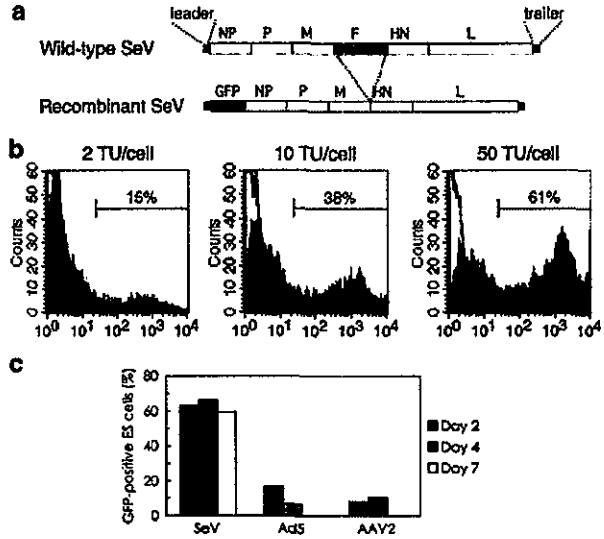

Figure 1 High-level transgene expression in cynomolgus ES cells after infection with SeV vector. (a) Schematic diagrams of the wild-type SeV genome and recombinant F-defective SeV carrying the GFP gene (SeV vector in this study). The SeV genome is 15 384 nucleotides long and its genes (NP, P, M, F, HN, and L) are in order from 3′ to 5′ in the negative-strand RNA. In the SeV vector, the entire fusion (F) gene was removed and the GFP gene was introduced at a unique NotI site between the leader sequence and NP gene. (b) The GFP expression by the SeV vector in cynomolgus ES cells. Cynomolgus ES cells were infected with the SeV vector at 2, 10, and 50 TU/cell. The flow cytometric profiles at day-2 postinfection are shown in gray. The white areas indicate uninfected ES cells. The fractions of GFP-positive cells are indicated. (c) The GFP expression levels in cynomolgus ES cells infected with the SeV (50 TU/cell), adenovirus serotype 5 (Ad5, 3.4×10^2 g.c./cell), and AAV serotype 2 (AAV2, 2.4×10^4 g.c./cell) vectors. The fractions of GFP-positive cells were examined by flow cytometry at 2, 4, and 7 days postinfection.

We plucked fluorescent ES cell colonies under a fluorescent microscope once at 1 month after infection and propagated them. After this selection procedure, approximately 90% of the ES cells expressed GFP (Figure 2a and b) and the high-level expression was stable for a year as assessed by flow cytometry (Figure 2c, upper). The mean fluorescence intensity per cell was also stable (Figure 2c, lower), indicating that the replicating vector genome was almost equally delivered to each cell of all progeny. The self-replication of the SeV vector in infected cells was confirmed by RNA-PCR that amplified the viral RNA genomic sequence (Figure 3a). The GFP cDNA sequence, however, could not be detected by DNA-PCR in the infected cells (Figure 3b), indicating that no DNA phase was involved in the GFP expression.

Pluripotency of infected ES cells

The SeV-infected, fluorescent cynomolgus ES cells were able to form fluorescent tumors when transplanted into immunodeficient mice (Figure 4a–c). The fluorescence was observed uniformly by fluorescent microcopy (Figure 4d and e). The tumors consisted of all three embryonic germ layer cells (Figure 4f–i). Thus, the SeV-infected ES cells were capable of forming teratomas and the SeV infection did not spoil the pluripotency of ES cells. The infected, fluorescent cynomolgus ES cells were also able to generate fluorescent embryoid bodies (Figure 5a and b), MAP-2-positive neurons (Figure 5c), clonogenic hematopoietic colonies (Figure 5d and e), and mature functional (NBT test-positive) neutrophils (Figure 5f and g), all of which fluoresced. In addition, the GFP expression levels were not decreased during the teratoma formation or differentiation, indicating that no 'silencing' of the transgene occurred.

Drug-inducible reduction of transgene expression

Next, we examined whether ribavirin inhibits the replication and transcription of the SeV vector resulting in a reduction of transgene expression. We first used a rhesus monkey kidney cell line (LLC-MK2) to test the effect of ribavirin on the replication and transcription of the SeV vector. LLC-MK2 is a standard control cell line for SeV infection. Ribavirin was added at various concentrations 2 days after the infection. The formation of viral particles quantified by the hemagglutination assay decreased drastically upon the addition of ribavirin (Figure 6a). The decrease was dependent on the dose of ribavirin. The GFP expression was also depressed dose-dependently (Figure 6b). Thus, ribavirin dose-dependently inhibits the replication and transcription of the SeV vector in LLC-MK2 cells. The toxicity associated with ribavirin was not observed in LLC-MK2 cells.

We then examined the effect of ribavirin on SeV-infected, fluorescent cynomolgus ES cells. The addition of ribavirin also resulted in a dose-dependent reduction of GFP expression in the cells (Figure 6c). Although the GFP expression was almost completely inhibited after a 3-day exposure with 4 mM of ribavirin, the cells could not be propagated thereafter. Ribavirin at high concentrations (>1 mM) hampered the proliferation of cynomolgus ES cells. With lower concentrations (0.5–0.75 mM) of ribavirin, the GFP expression level decreased by half. After the discontinuation of ribavirin treatment, the cells could be propagated and nearly regained the original level of GFP expression. The undifferentiated cell fractions were unchanged after the discontinuation as assessed by alkaline phosphatase and SSEA-4 staining (Figure 6d).

Discussion

There are several advantages in using SeV vectors over other vectors. (i) SeV vectors can infect nondividing, quiescent cells as well as dividing cells unlike oncoretroviral vectors.[7–11] Thus, they can be used to infect cells that are terminally differentiated as well as at various stages of differentiation, whether they are dividing or not. (ii) SeV vector-mediated gene transfer does not require a DNA phase. Thus, there is no concern about the unwanted integration of foreign sequences into the host genome unlike with oncoretroviral or lentiviral vectors. (iii) Transgene expression is stable even in dividing cells since the SeV vector replicates by itself in the cytoplasm of host cells. On the other hand, gene transfer using nonreplicating adenoviral and AAV vectors resulted in decreased levels of transgene expression in dividing cells over time, since the non-replicating transgene was